

NACA RM E51E29

E 51 E 87

TECH LIBRARY KAFB, NM  
0143199

NACA

# RESEARCH MEMORANDUM

DATA PRESENTATION OF FORCE CHARACTERISTICS OF SEVERAL  
ENGINE-STRUT-BODY CONFIGURATIONS AT

MACH NUMBERS OF 1.8 AND 2.0

By Robert T. Madden and Emil J. Kremzier

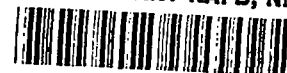
Lewis Flight Propulsion Laboratory  
Cleveland, Ohio

*Emil J. Kremzier*

NATIONAL ADVISORY COMMITTEE  
FOR AERONAUTICS

WASHINGTON  
August 14, 1951

319.98/13



0143199

NACA RM E51E29

~~CONFIDENTIAL~~

## NATIONAL ADVISORY COMMITTEE FOR AERONAUTICS

RESEARCH MEMORANDUM

## DATA PRESENTATION OF FORCE CHARACTERISTICS OF SEVERAL

## ENGINE-STRUT-BODY CONFIGURATIONS AT

## MACH NUMBERS OF 1.8 AND 2.0

By Robert T. Madden and Emil J. Kremzier

## SUMMARY

Lift, drag, and pitching-moment characteristics obtained from an investigation of several engine-strut-body combinations in the NACA Lewis 8- by 6-foot supersonic wind tunnel are presented for Mach numbers of 1.8 and 2.0 and a range of angle of attack from  $0^\circ$  to  $10^\circ$ . Data for the isolated body, isolated engine, and body-strut configurations are also presented for the same range of variable. The average Reynolds number based on body length was  $28 \times 10^6$ .

The results indicated decreases in minimum drag and lift curve slope with decreasing strut length. Decreases in minimum drag are also noted with rearward movement of the engines.

## INTRODUCTION

In the design of supersonic aircraft, much work has been done on the determination of the aerodynamic characteristics of isolated components such as the wing, engine, and fuselage, whereas little information is available on the characteristics of a complete configuration where aerodynamic interference effects exist. As part of a general program to study the interference problem associated with missile configurations, an investigation of the aerodynamic characteristics of an engine-strut-body combination was undertaken. With this general type of configuration, the external aerodynamic characteristics and the engine characteristics are influenced by the relative location of the engine with respect to the body.

The investigation was conducted in the NACA Lewis 8- by 6-foot supersonic wind tunnel to determine experimentally the lift, drag, and pitching-moment characteristics of the engine-strut-body combination for various engine locations. Characteristics of the isolated body, isolated engine, and the body with two struts are also included. Data

PERMANENT

SECRET

~~CONFIDENTIAL~~

55-677

were obtained at Mach numbers of 1.8 and 2.0 for an angle of attack range from  $0^\circ$  to  $10^\circ$  at a Reynolds number of approximately  $28 \times 10^6$  based on the body length.

In order to expedite publication, the data obtained from these tests are presented in this report without analysis.

### SYMBOLS

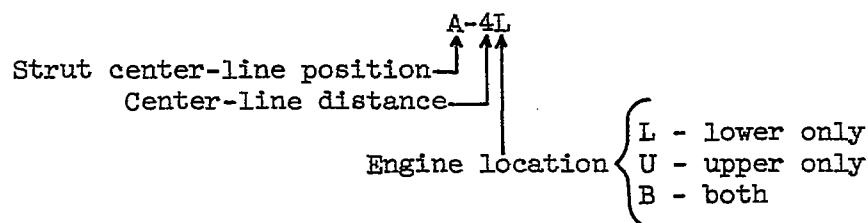
The following symbols are used in this report:

b	local body radius
$C_D$	drag coefficient, $D/q_0 S_m$
$C_L$	lift coefficient, $L/q_0 S_m$
$C_M$	pitching-moment coefficient, $G_{35}/q_0 S_m l$
$C_{M,1}$	pitching-moment coefficient, $G_1/q_0 S_m l$
D	drag
G	pitching moment
L	lift
l	body length
$M_0$	free-stream Mach number
$q_0$	free-stream dynamic pressure
$S_m$	maximum cross-sectional area of body
x	longitudinal distance from station 0 to local station on body
$\alpha$	angle of attack, deg

### Subscripts:

0	free stream
1	engine-inlet entrance
35	body station 35

Configuration designation (fig. 1):



#### APPARATUS AND PROCEDURE

The investigation was conducted in the 8- by 6-foot supersonic wind tunnel at Mach numbers of 1.8 and 2.0 for nominal angles of attack of  $0^\circ$ ,  $2^\circ$ ,  $4^\circ$ ,  $6^\circ$ ,  $8^\circ$ , and  $10^\circ$ .

A sketch of the model which utilized the NACA RM-10 body is shown in figure 1. The model was sting mounted on a tunnel support system similar to that described in reference 1. Force measurements were obtained from a three-component strain-gage balance located within the body. The moment center of the balance was located at station 35. A modified support system was used for the determination of the characteristics of the isolated engine (fig. 2).

The tables in figure 1 indicate the strut center-line positions and body-engine center-line distances that were investigated using both engines, an engine above, or an engine below the body. Figure 3 shows scale drawings of the various two-engine configurations investigated. Single-engine configurations were identical to these, with either the upper or lower engine removed. The engines were mounted such that their center lines were in the angle of attack plane, a vertical plane through the center line of the body. Engine mounting struts were fixed with respect to the engine, and engine location was varied by varying the fore and aft position of the struts on the body and by changing the strut length. Investigations of the isolated body, isolated engine, and body-strut configurations were also conducted to determine the characteristics of the individual components. The body-strut configurations were investigated with two different strut lengths of 8.61 and 19.72 inches measured from the body center line to the tip.

Pressure instrumentation on each of the engines consisted of a mass-flow rake with seven total-pressure and two static-pressure tubes located at the inlet entrance, three base-pressure orifices, and two outlet nozzle static-pressure orifices. The body instrumentation included two base-pressure orifices and a static-pressure tube within the balance chamber. For the isolated engine run, the original pressure instrumentation was removed and replaced by base-pressure orifices on the engine shell and exit plug, and nozzle static-pressure orifices on the exit plug.

Force coefficients presented in this report are based on the maximum cross-sectional area of the body and moment coefficients are based on the body length and maximum cross-sectional area. All moments are taken about station 35 with the exception of the isolated engine moments, which were taken about the engine-inlet entrance. The force and moment coefficients presented do not include the axial force due to the flow through the engines or the base force resulting from the difference in base pressures from free-stream static. The coefficients do, however, include the internal normal force at angle of attack resulting from turning the flow at the inlet entrance from the local free-stream direction to that of the engine axis.

The engines were designed to operate without burning and with the normal shock downstream of the inlet entrance for all test conditions so that flow conditions of the configurations would not be complicated by variations in mass-flow spillage around the outside of the inlets.

#### PRESENTATION OF DATA

Lift, drag, and moment coefficients are presented in figures 4, 5, and 6 for the two-engine, lower engine, and upper engine configurations, respectively, while figures 7, 8, and 9 present the characteristics of the isolated body, isolated engine, and body with two struts.

The following table gives values of external drag coefficient for the isolated engine as determined from two different methods at zero angle of attack and Mach numbers of 1.8 and 2.0. The  $C_D$  (friction) values were obtained from measurements on a boundary-layer rake installed at the base of the model. Reference 2 was used to obtain  $C_D$  (pressure). The next column shows the values of external drag coefficient resulting from  $C_D$  (friction) +  $C_D$  (pressure) and the last column gives values of  $C_D$  (balance) determined from the balance measurements.

$M_0$	$C_D$ (friction)	$C_D$ (pressure)	$C_D$ (pressure + friction)	$C_D$ (balance)
1.8	0.0270	0.0084	0.0354	0.0392
2.0	.0266	.0076	.0342	.0355

The discrepancy between the values of external drag coefficient obtained by the two methods is considered to be an indication of the accuracy of the drag coefficients presented. The largest discrepancy is about 10 percent and occurs at a Mach number of 1.8. The  $C_D$  (balance) for the isolated engine is inherently subject to the largest error of any of the configurations investigated because the drag forces recorded by the balance include the external drag in addition to a

large internal and base drag which must be subtracted from the balance measurements. Discrepancies noted from a similar drag comparison of the isolated body (reference 3) were about 3 percent.

Scatter or deviation of individual data points from the mean faired curves presented is considered to be an indication of the precision involved in obtaining and reducing the data.

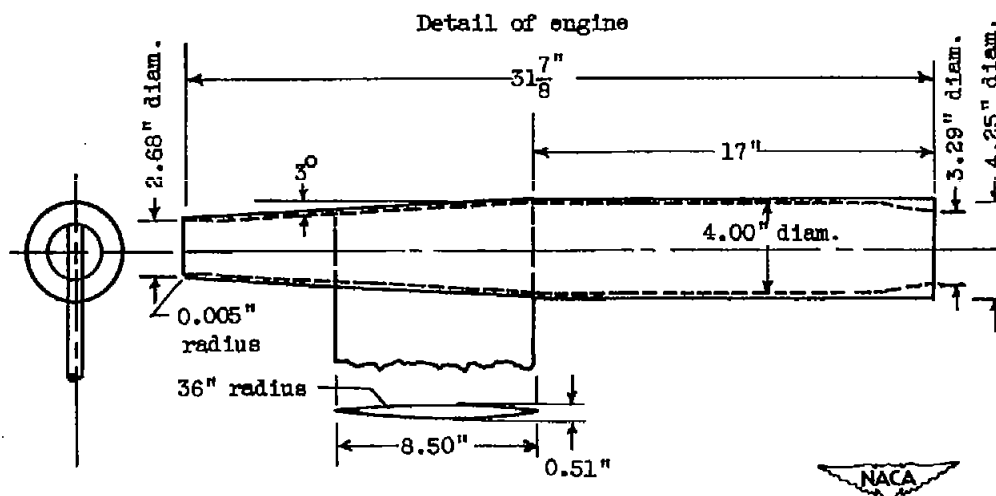
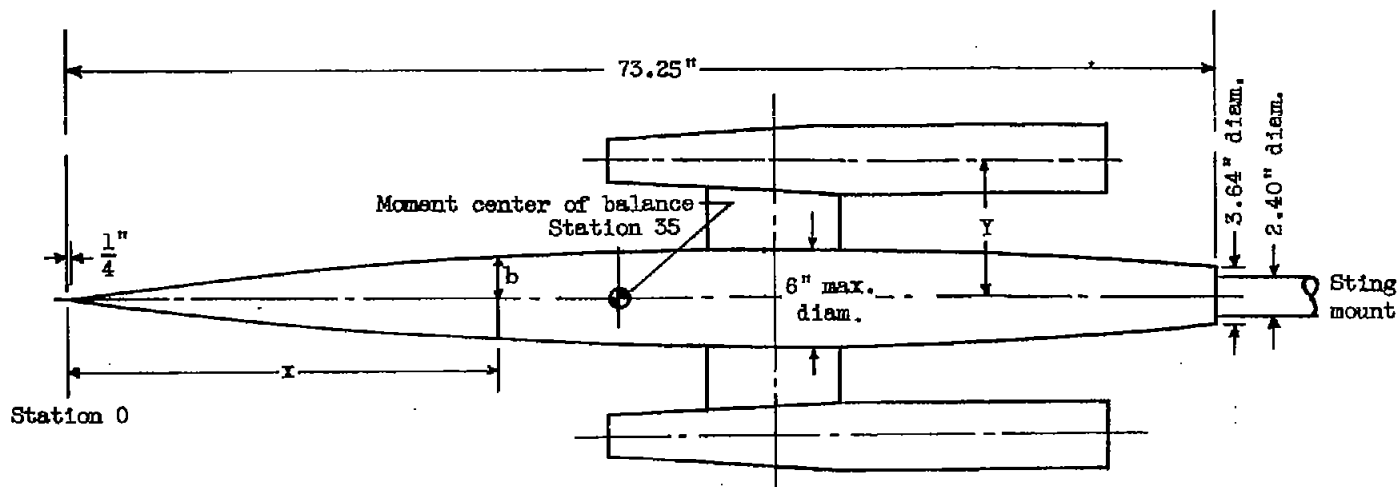
In general the characteristics of the engine-strut-body configurations show smooth and consistent variations with angle of attack. Several deviations from the consistent variations can be noted, however, particularly in the pitching-moment coefficient at angles of attack above  $6^\circ$  for the upper engine configurations with center-line distances 1 and 2. These deviations result from engine-body interference and become more pronounced as the engine is moved rearward. At the C strut position, the deviations are a maximum and may result in part from support sting interference because of the large amount of overhang of the engine downstream of the body base.

A general comparison of the results obtained from the tests of all configurations indicates decreases in both the minimum-drag coefficient and the lift-curve slope with decreasing strut length. It is also apparent that the minimum-drag coefficient decreases as the engine is moved rearward.

Lewis Flight Propulsion Laboratory,  
National Advisory Committee for Aeronautics,  
Cleveland, Ohio.

#### REFERENCES

1. Luidens, Roger W., and Simon, Paul C.: Aerodynamic Characteristics of NACA RM-10 Missile in 8- by 6-Foot Supersonic Wind Tunnel at Mach Numbers from 1.49 to 1.98. I - Presentation and Analysis of Pressure Measurements (Stabilizing Fins Removed). NACA RM E50D10, 1950.
2. Jack, John R.: Theoretical Wave Drags and Pressure Distributions for Axially Symmetric Open-Nose Bodies. NACA TN 2115, 1950.
3. Esenwein, Fred T., Obery, Leonard J., and Schueller, Carl F.: Aerodynamic Characteristics of NACA RM-10 Missile in 8- by 6-Foot Supersonic Wind Tunnel at Mach numbers from 1.49 to 1.98. II - Presentation and Analysis of Force Measurements. NACA RM E50D28, 1950.



Body defined by equation:

$$b = \frac{x}{15} \left[ 2 - \frac{x}{45} \right]$$

$$0 \leq x \leq 73.25$$

Strut center-line position	$\bar{x}$ (in.)
A	45
B	57
C	67.5
Center-line distance	$\bar{y}$ (in.)
1	5.12
2	6.38
3	8.50
4	10.62

**Figure 1. = Sketch of engine-body configuration.**

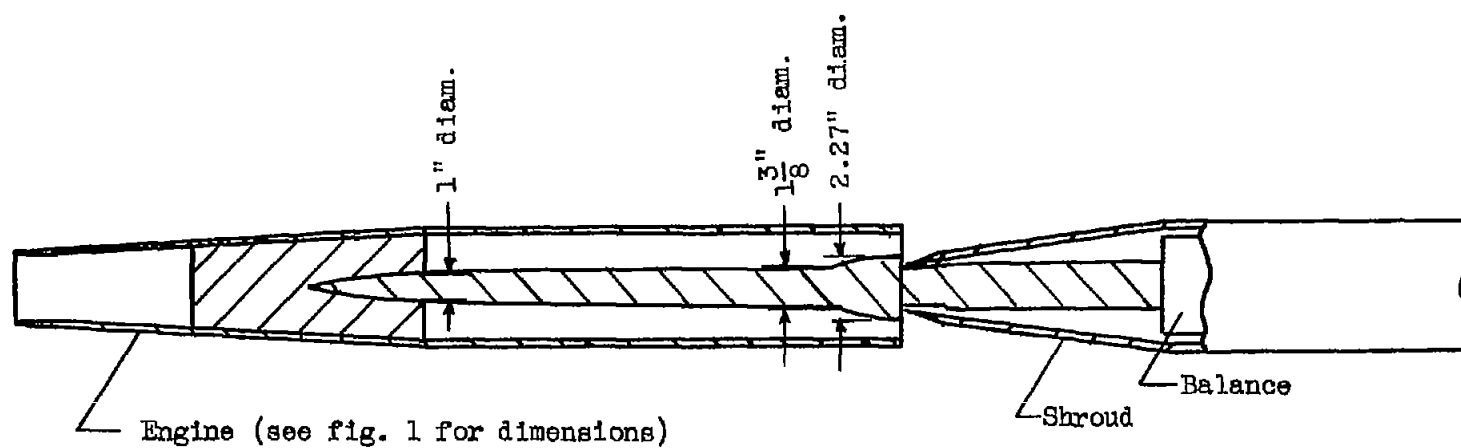
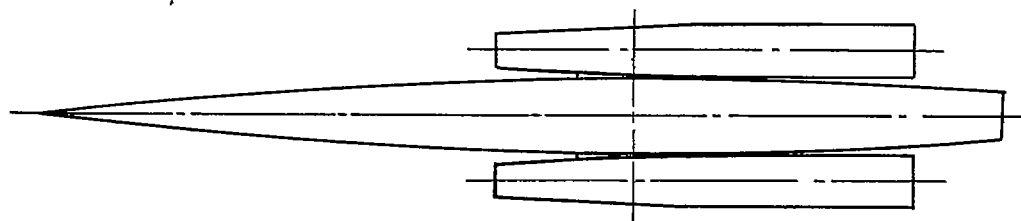
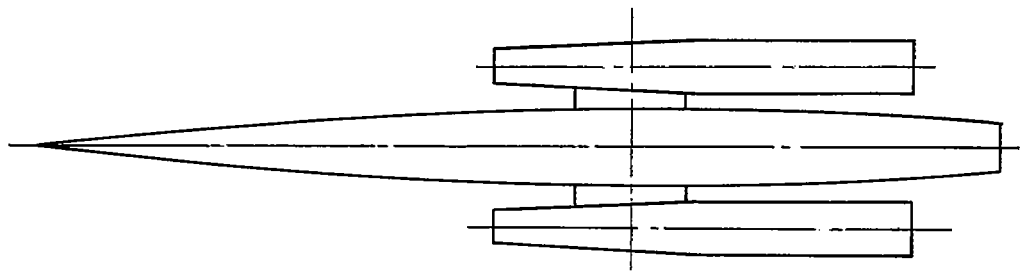


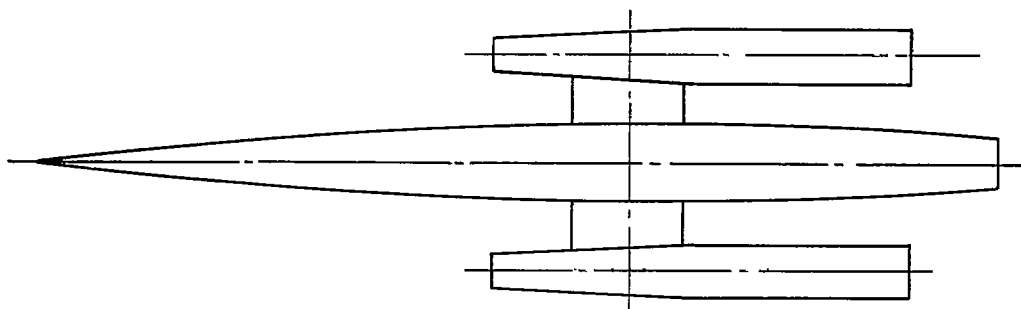
Figure 2. - Sketch showing support system for isolated engine test.



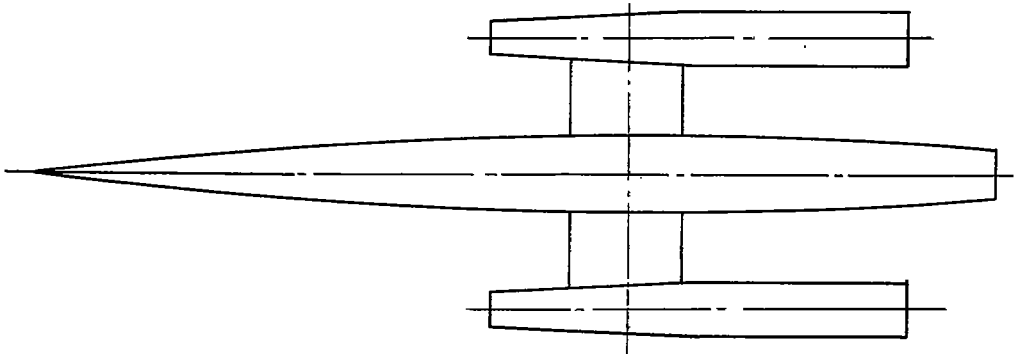
Configuration A-1B



Configuration A-2B



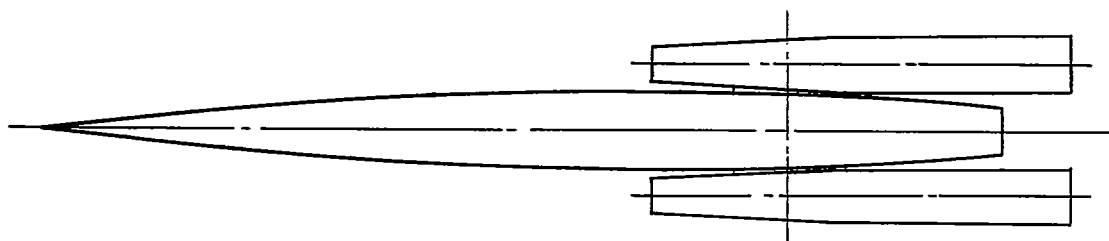
Configuration A-3B



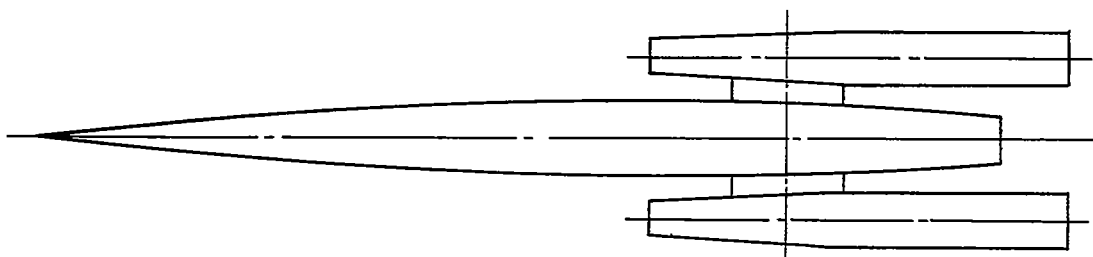
Configuration A-4B

(a) Position A.

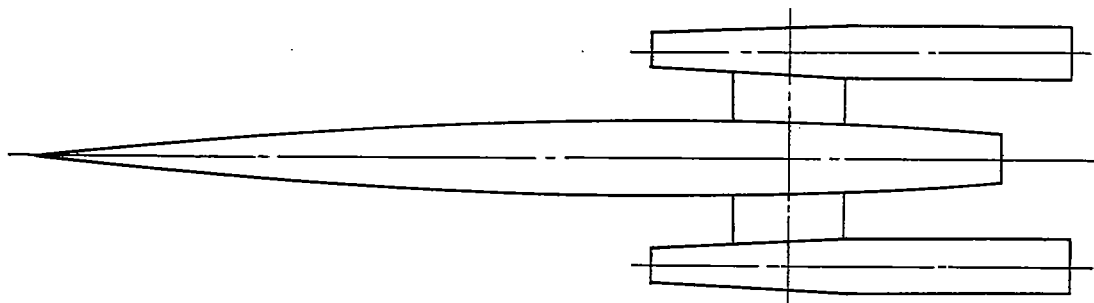
Figure 3. - Scale drawing of two-engine configurations showing various engine locations investigated.



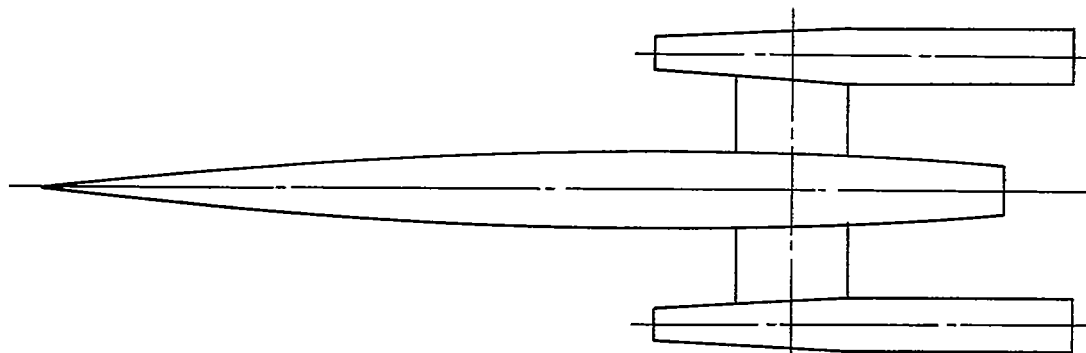
Configuration B-1B



Configuration B-2B



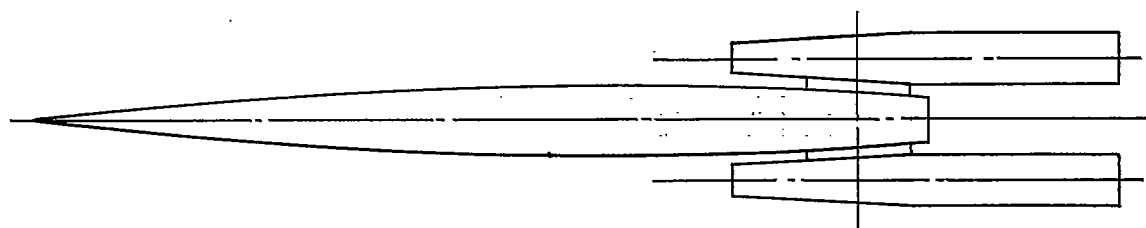
Configuration B-3B



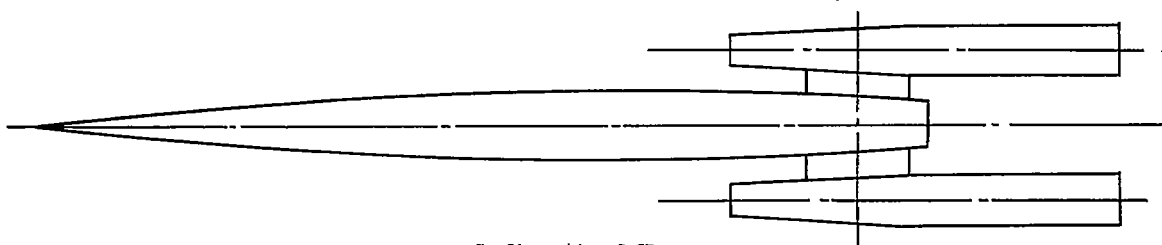
Configuration B-4B.

(b) Position B.

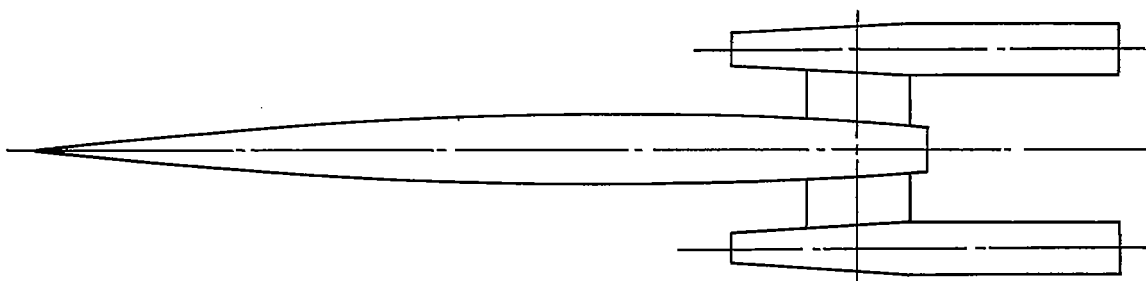
Figure 3. - Continued. Scale drawing of two-engine configurations showing various engine locations investigated.



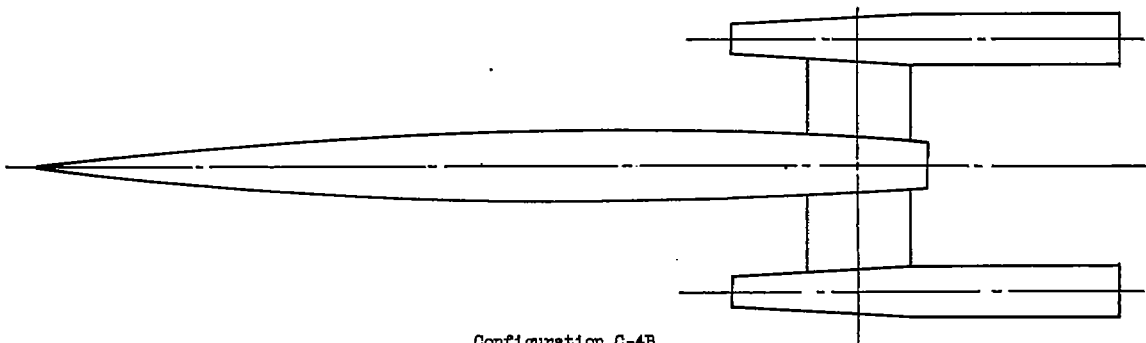
Configuration C-1B



Configuration C-2B



Configuration C-3B



Configuration C-4B

(c) Position C.

Figure 3. - Concluded. Scale drawing of two-engine configurations showing various engine locations investigated.

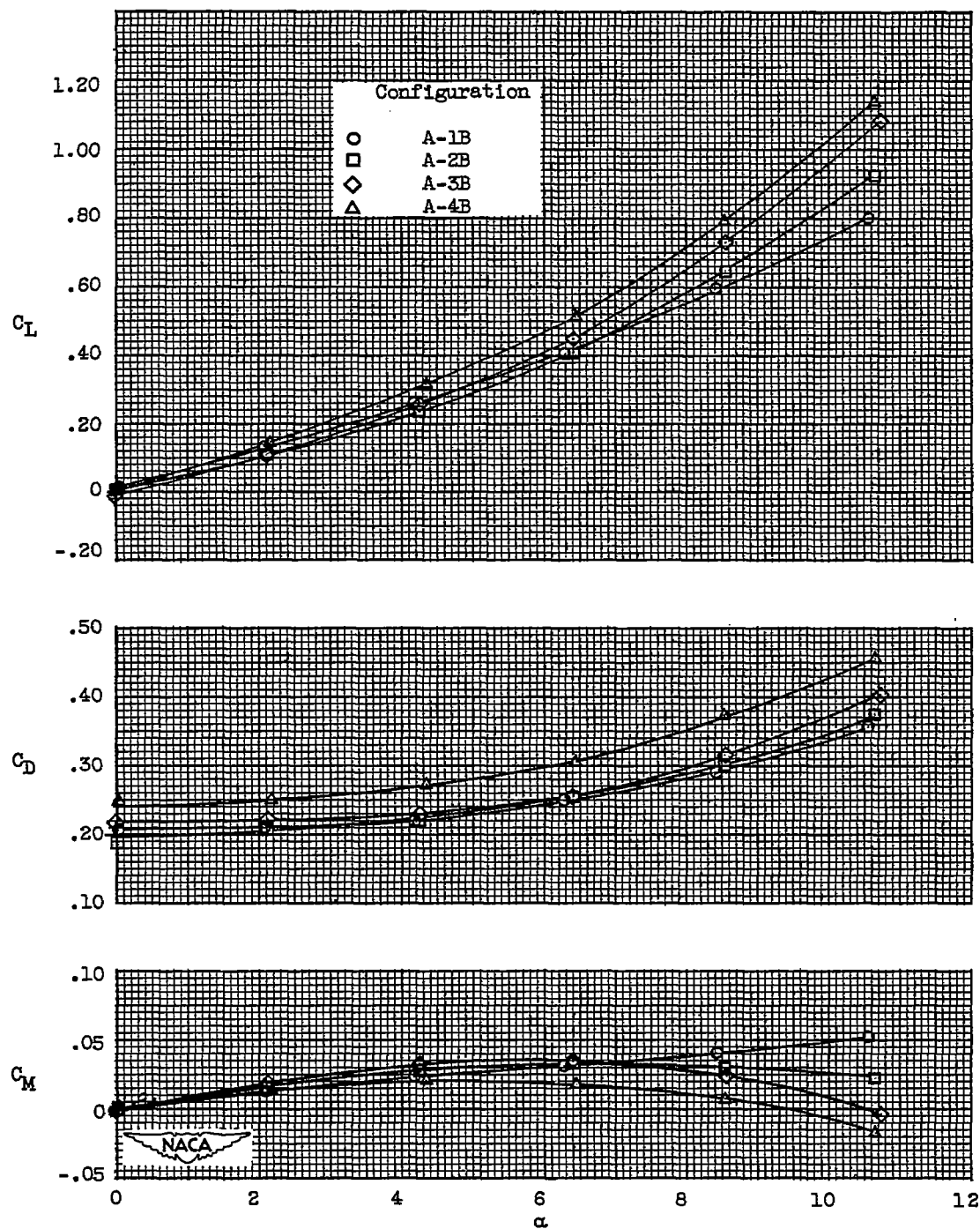
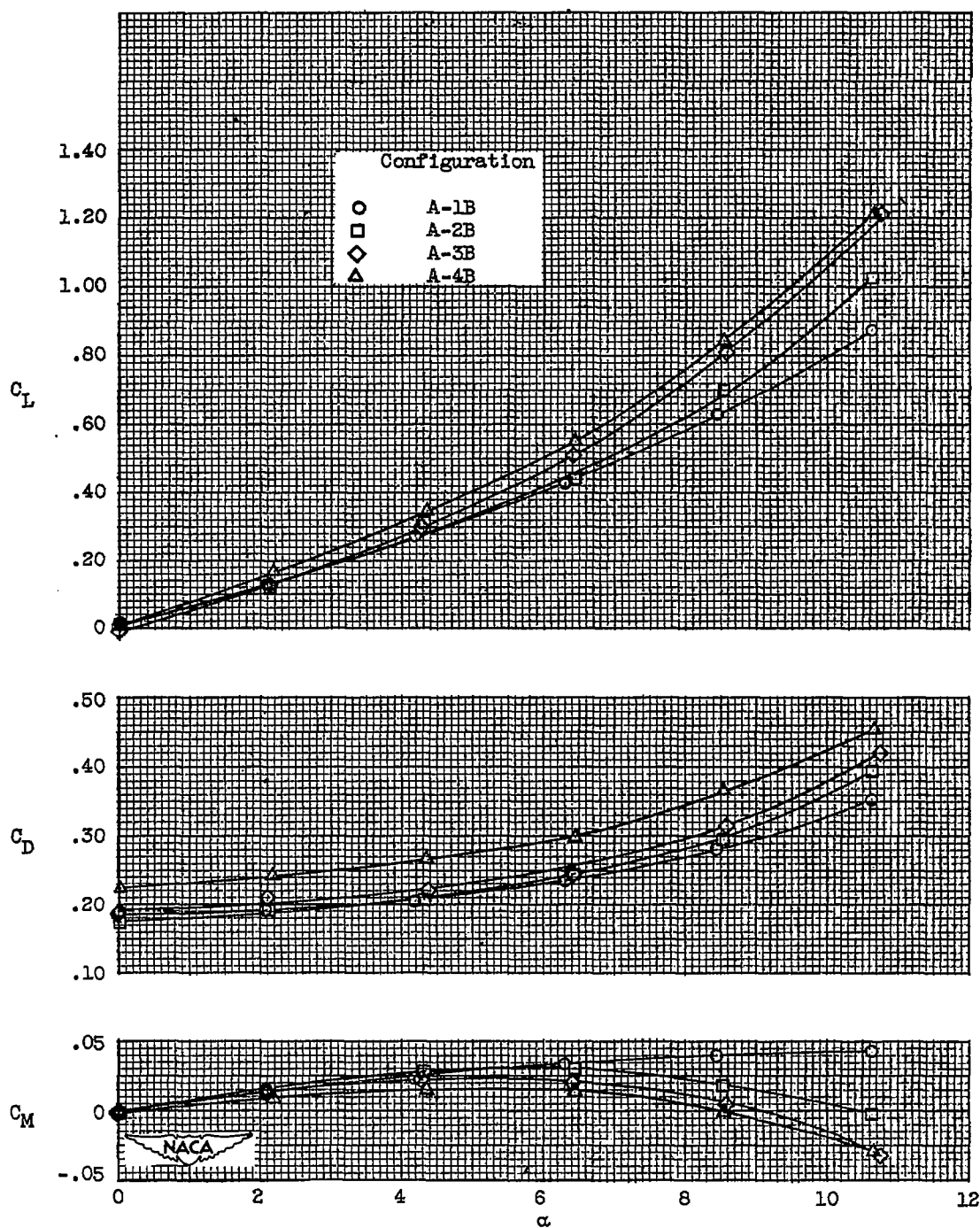
~~CONFIDENTIAL~~(a) Strut center-line position A.  $M_0$ , 1.8.

Figure 4. - Characteristics of configurations with two engines.

~~CONFIDENTIAL~~



(b) Strut center-line position A.  $M_0$ , 2.0.

Figure 4. - Continued. Characteristics of configurations with two engines.

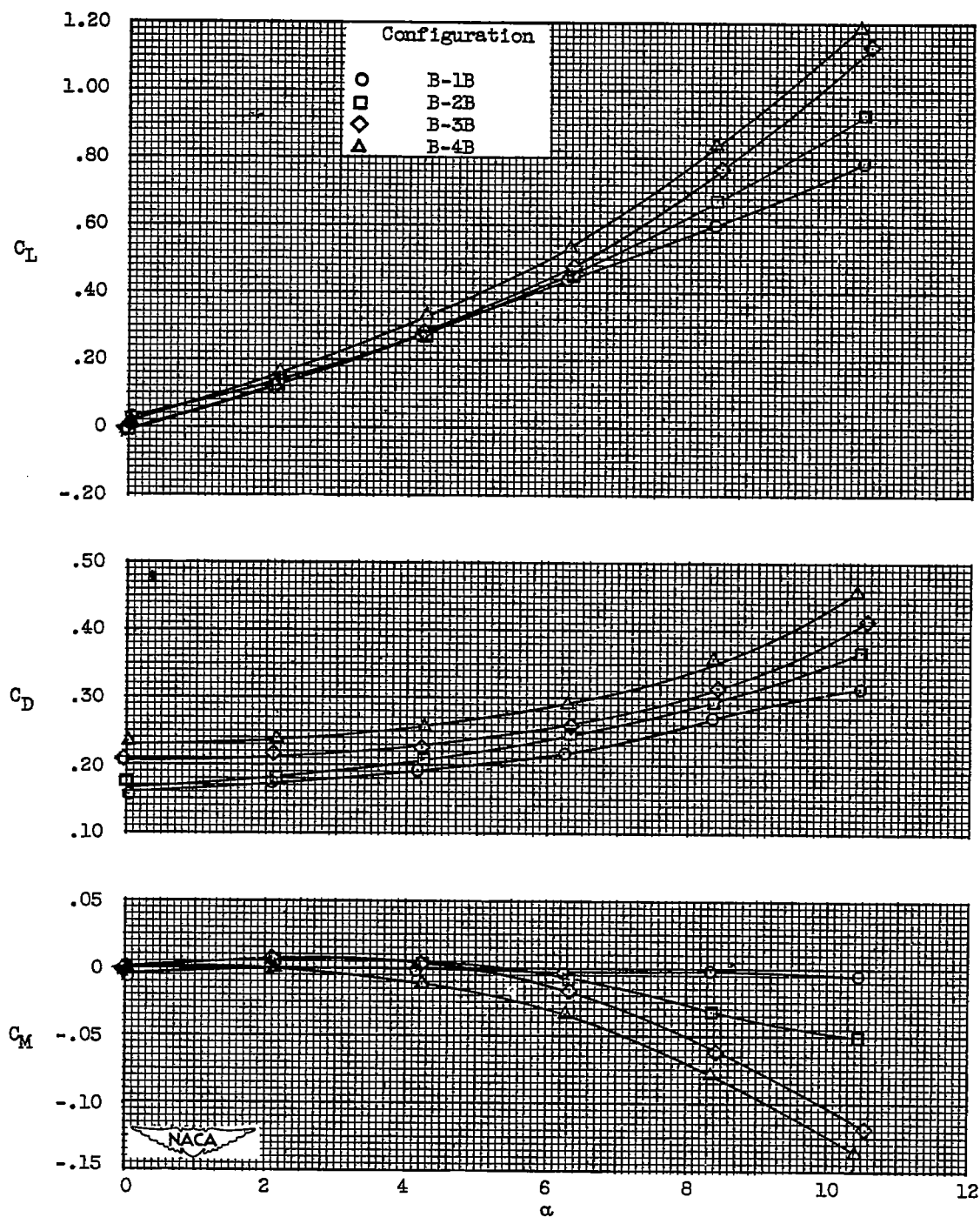
(c) Strut center-line position B.  $M_0$ , 1.8.

Figure 4. - Continued. Characteristics of configurations with two engines.

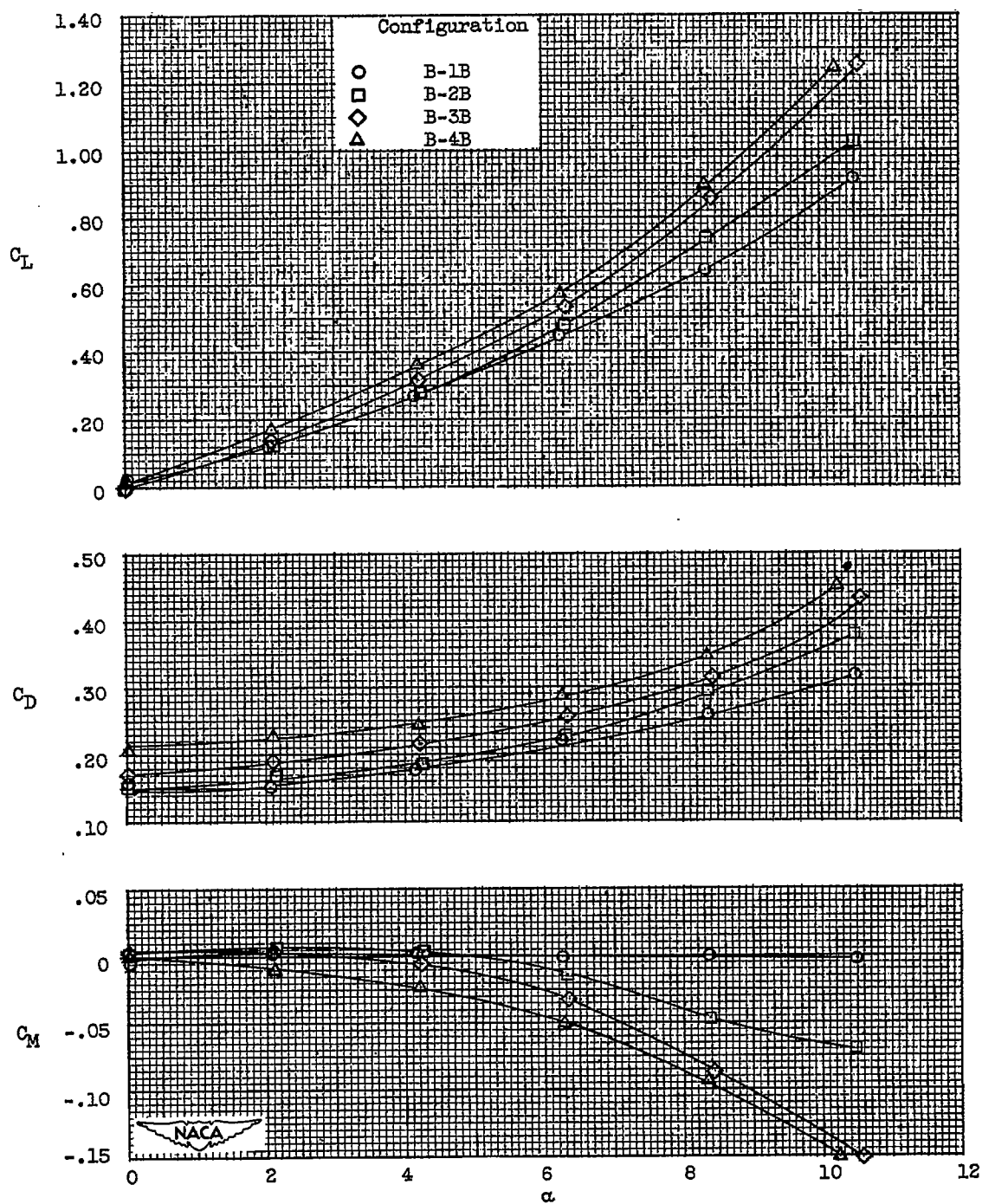
(d) Strut center-line position B.  $M_0$ , 2.0.

Figure 4. - Continued. Characteristics of configurations with two engines.

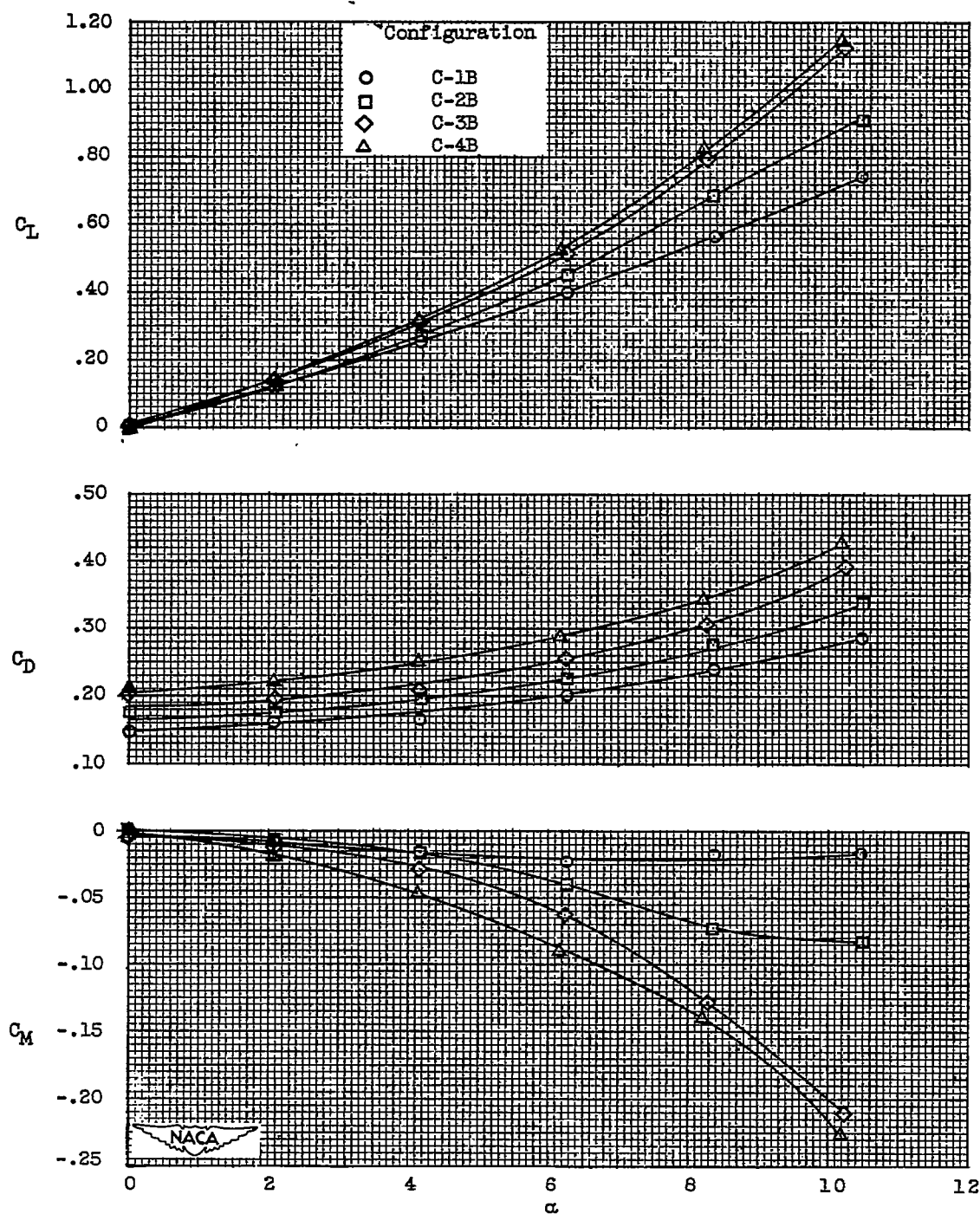
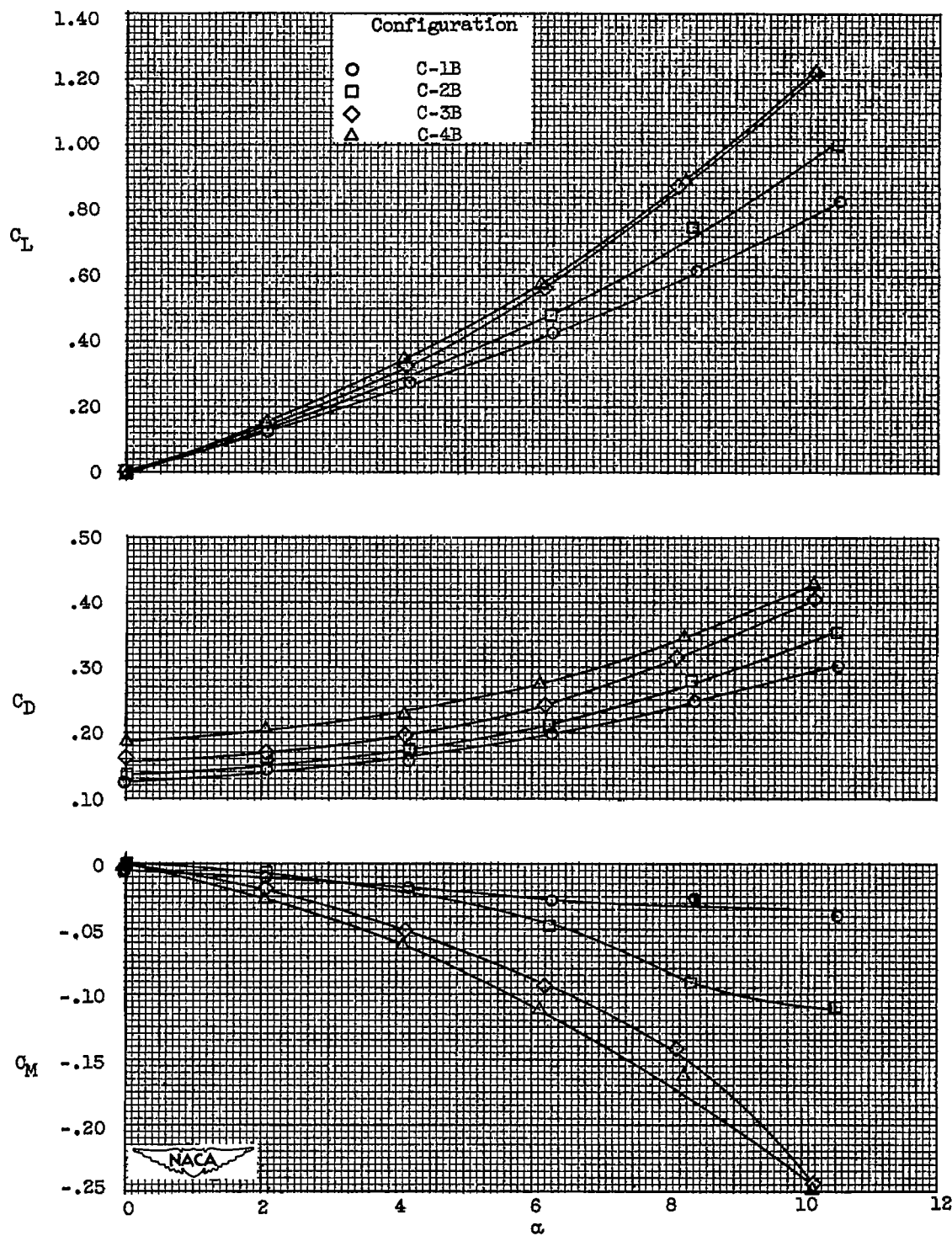
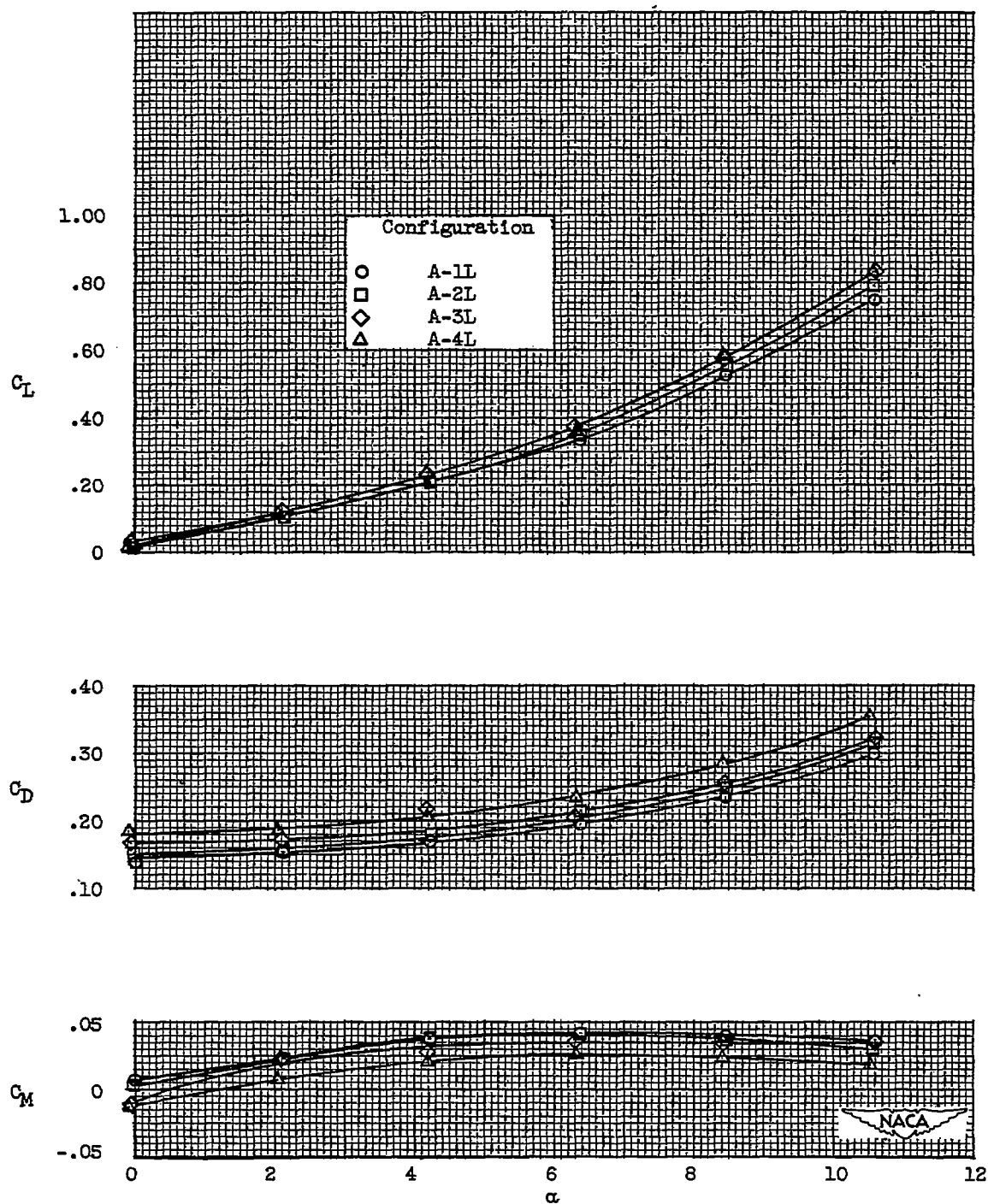
(e) Strut center-line position C.  $M_0$ , 1.8.

Figure 4. - Continued. Characteristics of configurations with two engines.



(f) Strut center-line position C.  $M_0$ , 2.0.

Figure 4. - Concluded. Characteristics of configurations with two engines.



(a) Strut center-line position A.  $M_0$ , 1.8.

Figure 5. - Characteristics of configurations with one engine below body.

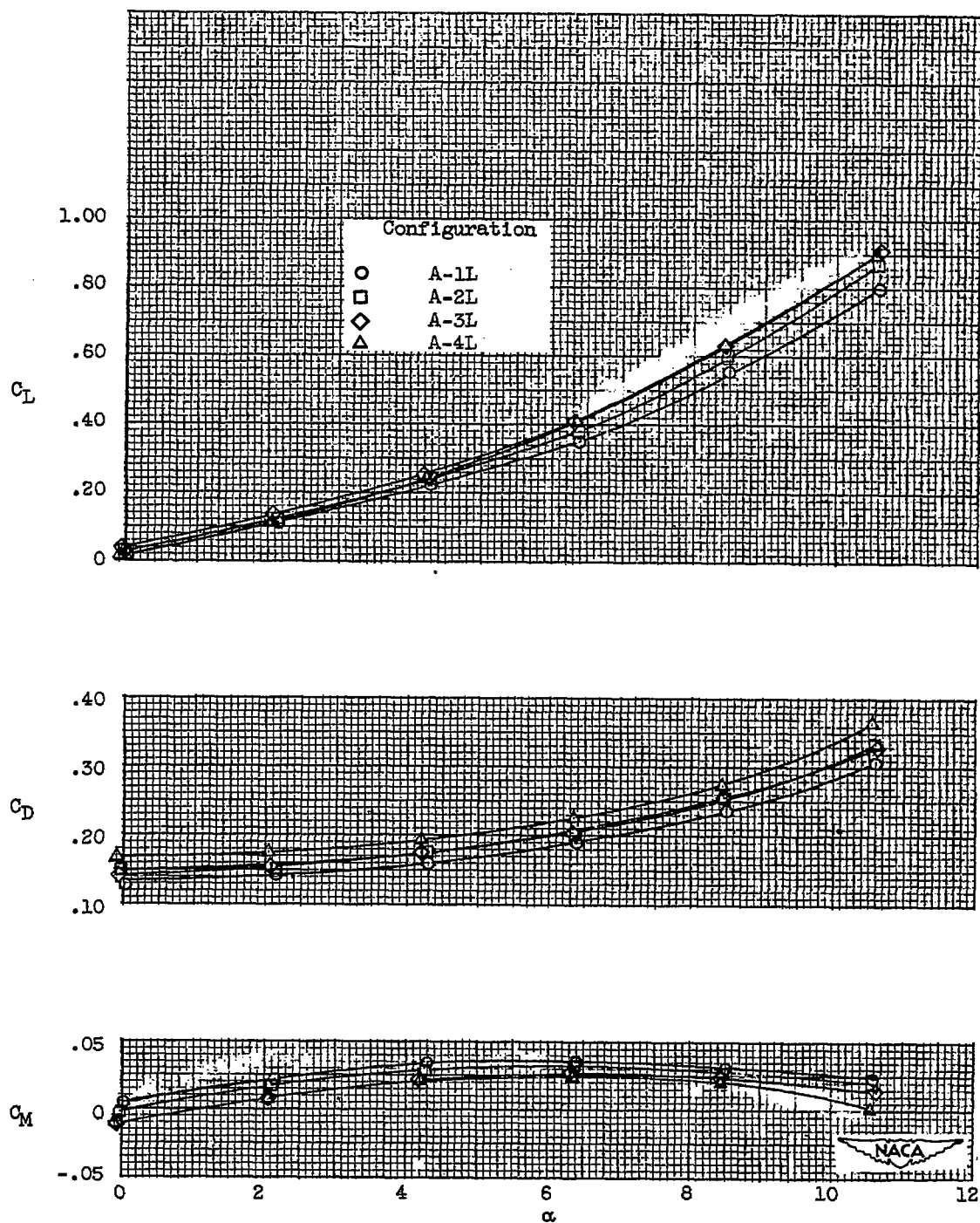
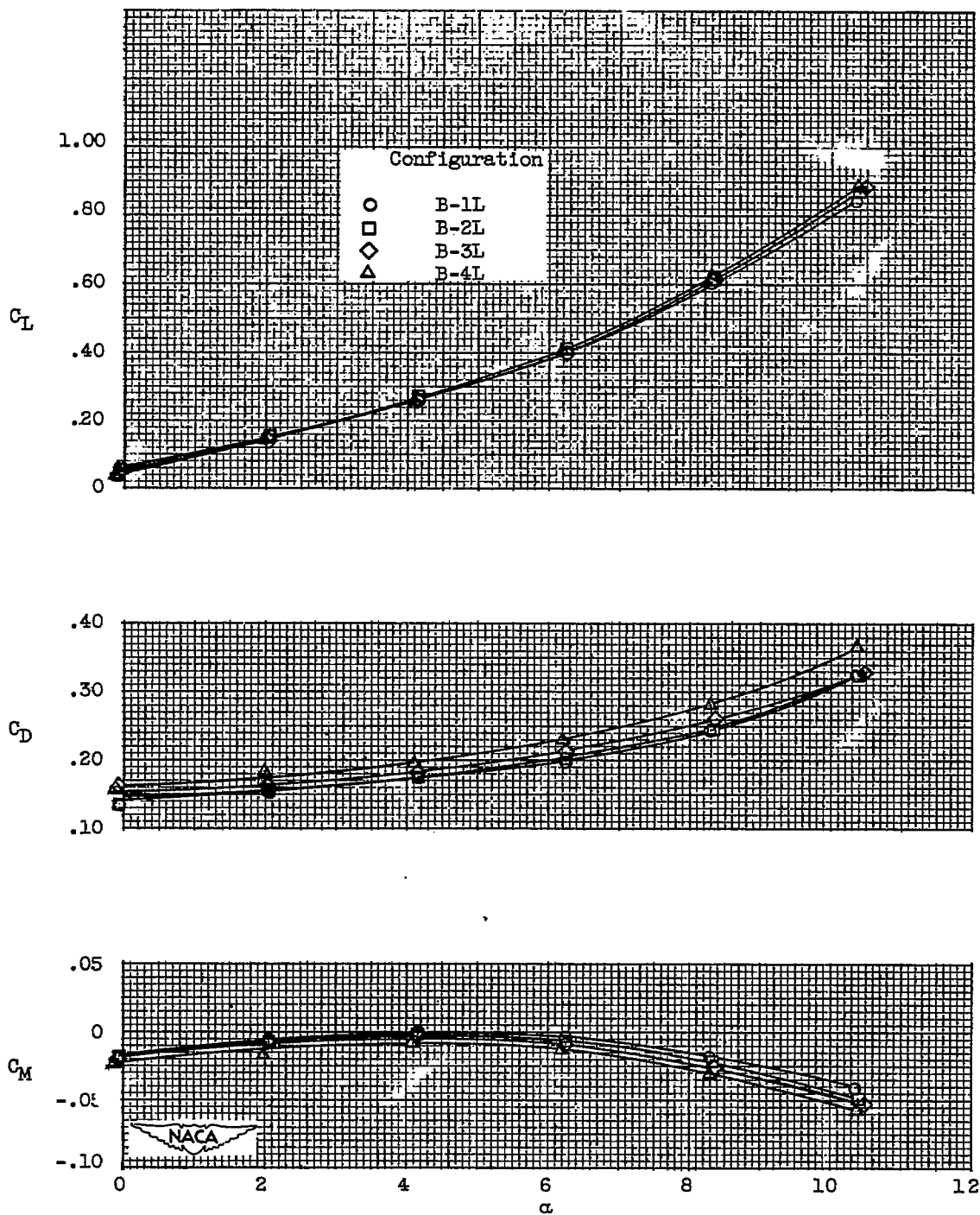
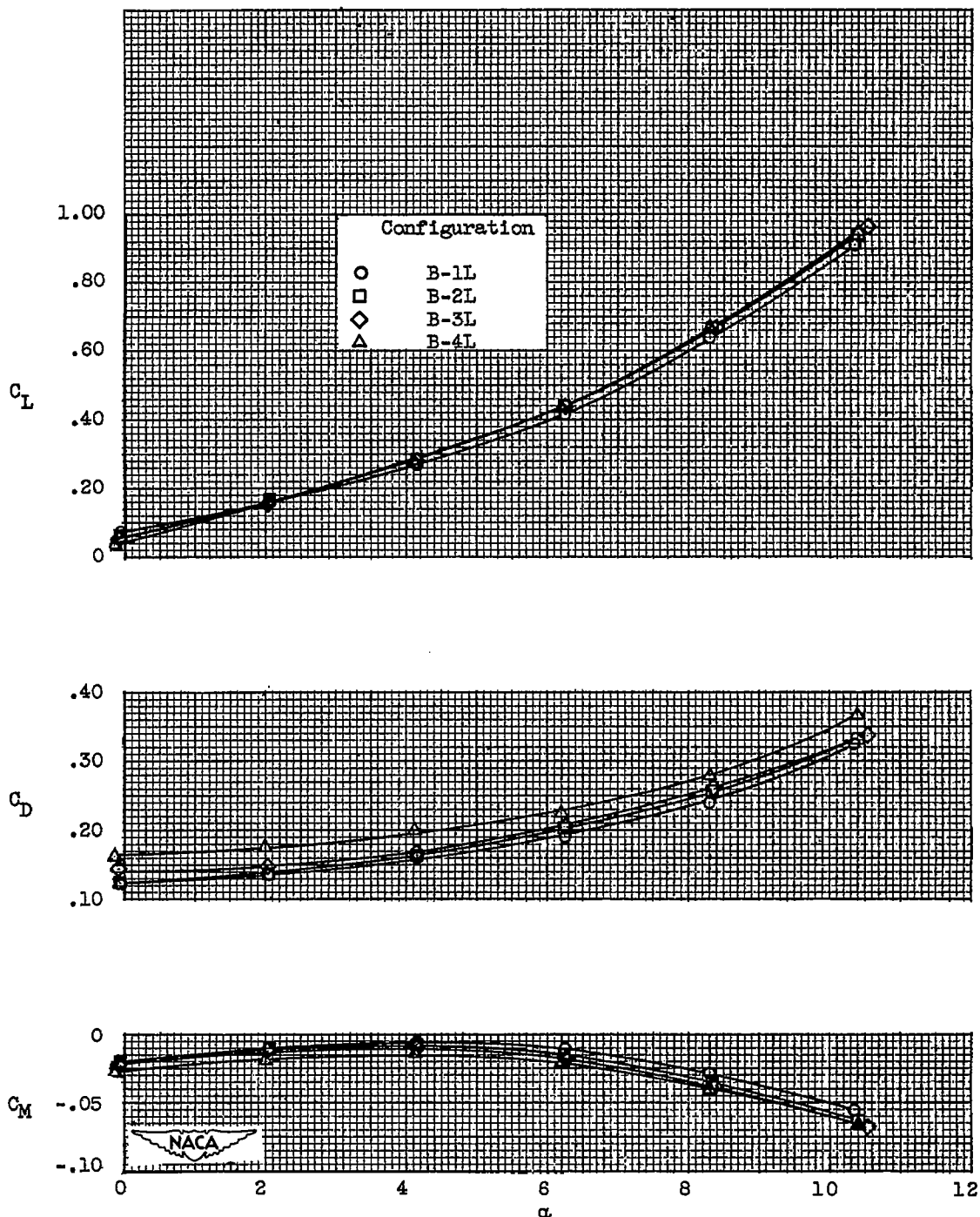
(b) Strut center-line position A.  $M_0$ , 2.0.

Figure 5. - Continued. Characteristics of configurations with one engine below body.



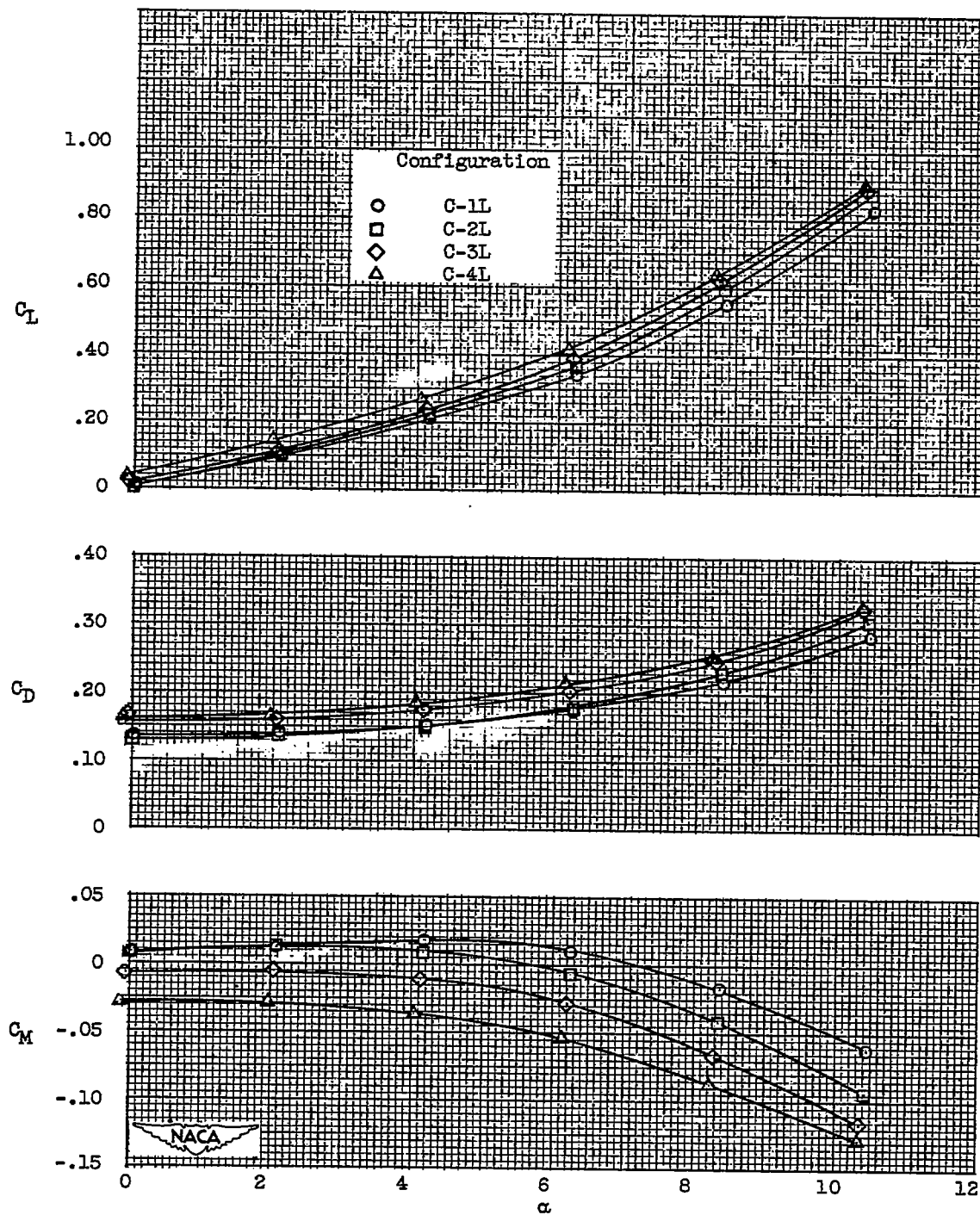
(c) Strut center-line position B.  $M_0$ , 1.8.

Figure 5. - Continued. Characteristics of configurations with one engine below body.



(d) Strut center-line position B.  $M_0$ , 2.0.

Figure 5. - Continued. Characteristics of configurations with one engine below body.



(e) Strut center-line position C.  $M_0$ , 1.8.

Figure 5. - Continued. Characteristics of configurations with one engine below body.

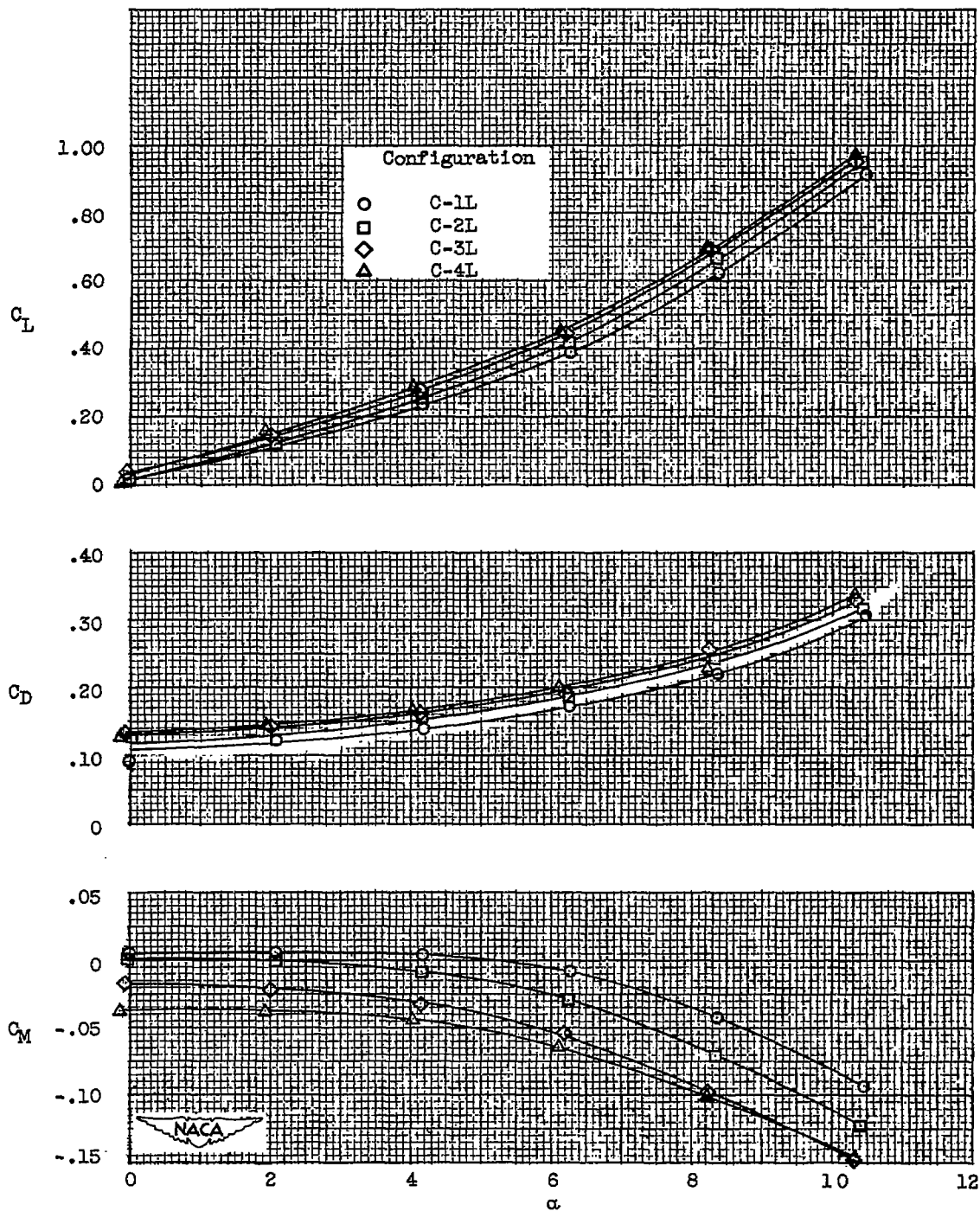
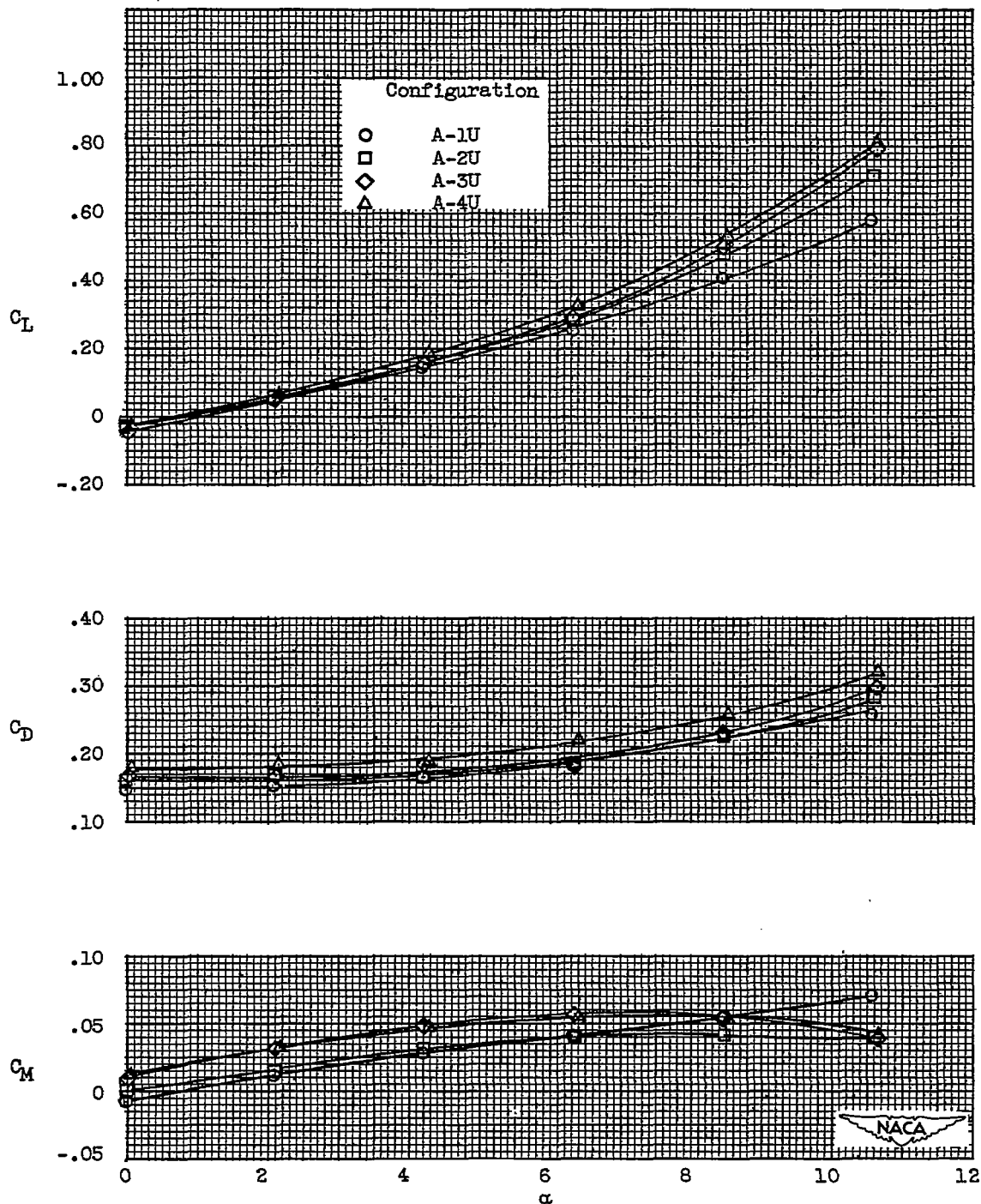
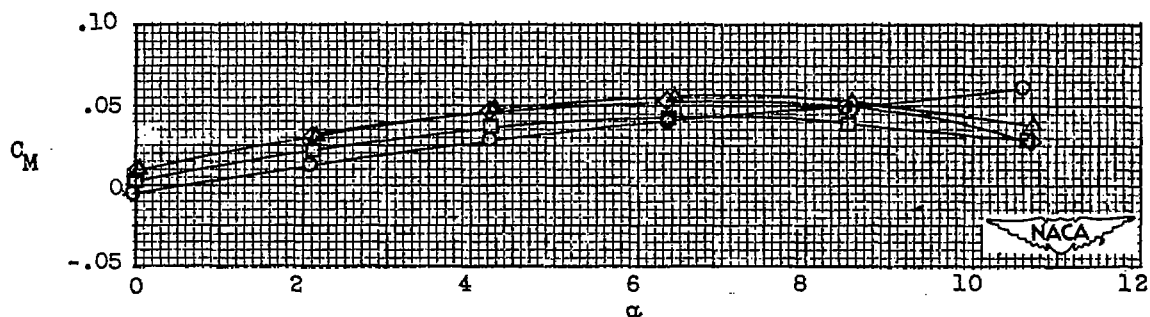
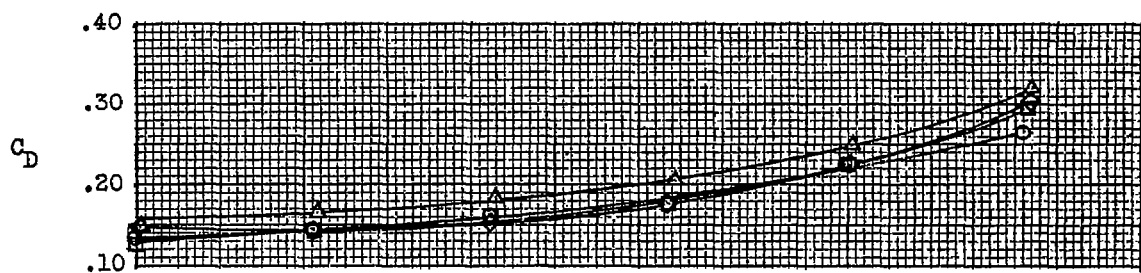
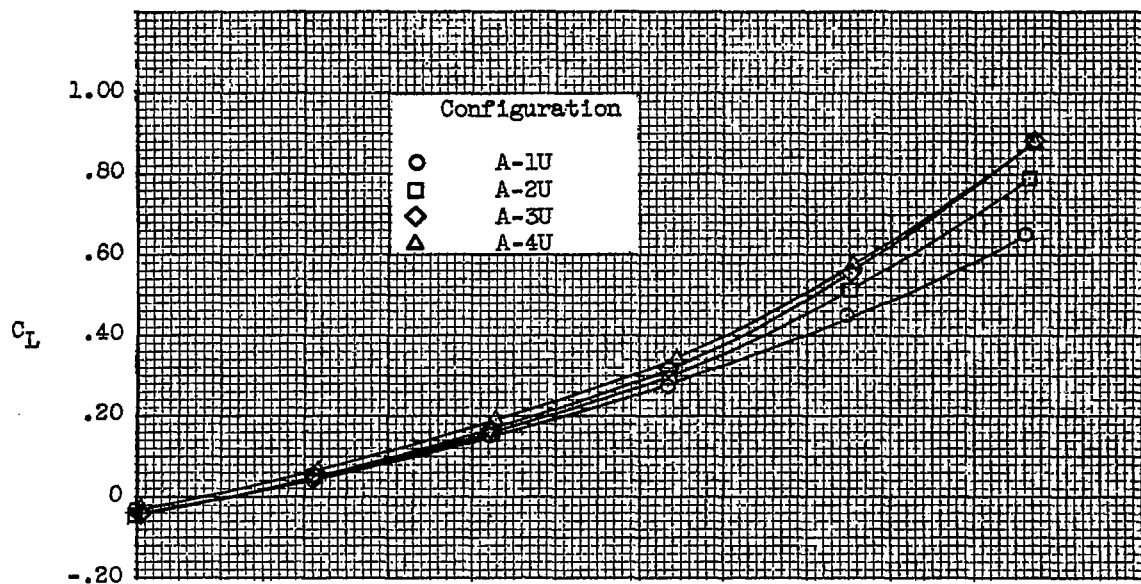
(f) Strut center-line position C.  $M_0$ , 2.0.

Figure 5. - Concluded. Characteristics of configurations with one engine below body.



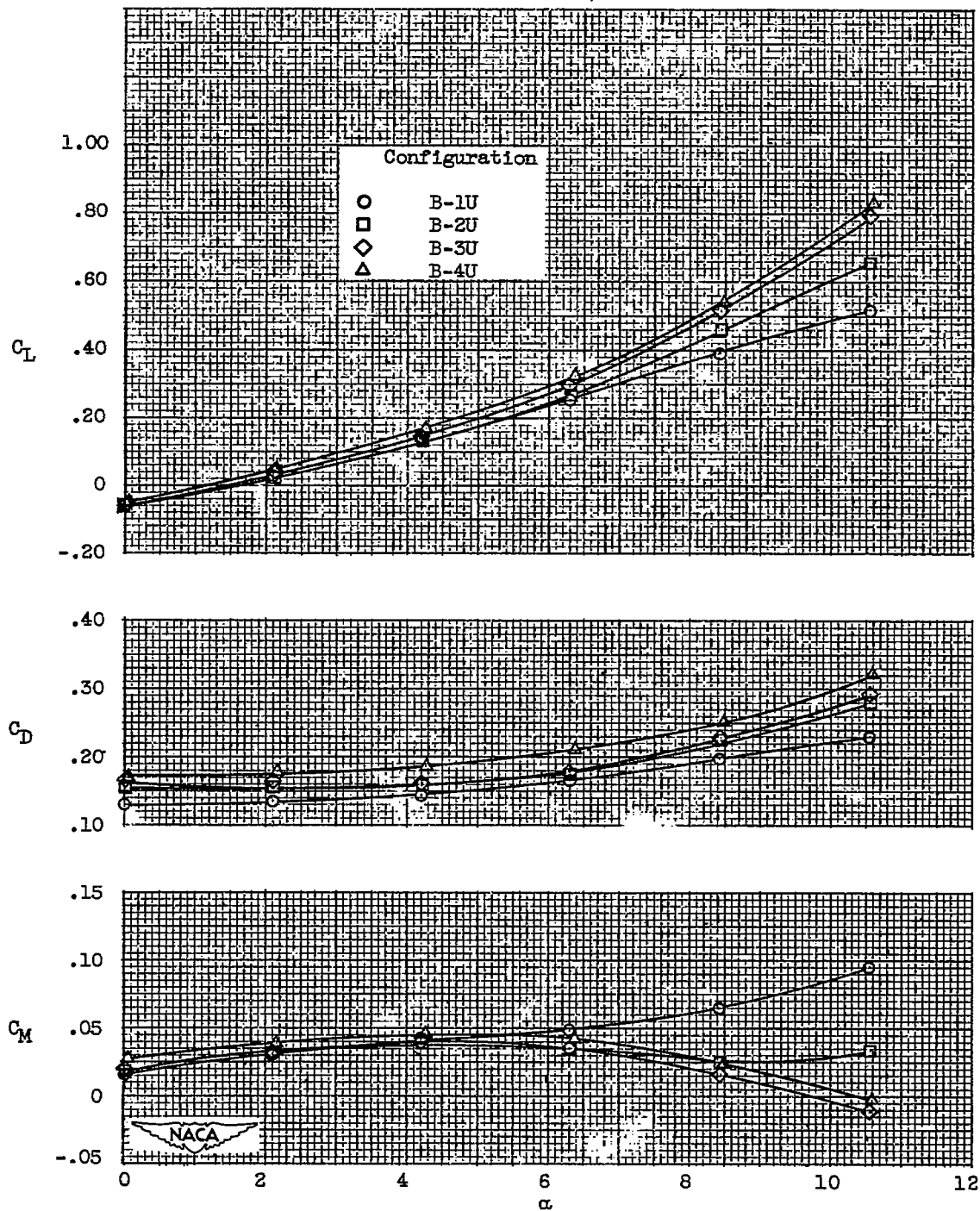
(a) Strut center-line position A.  $M_0$ , 1.8.

Figure 6. - Characteristics of configurations with one engine above body.



(b) Strut center-line position A.  $M_0$ , 2.0.

Figure 6. - Continued. Characteristics of configurations with one engine above body.



(c) Strut center-line position B.  $M_0, 1.8$ .

Figure 6. - Continued. Characteristics of configurations with one engine above body.

CONFIDENTIAL

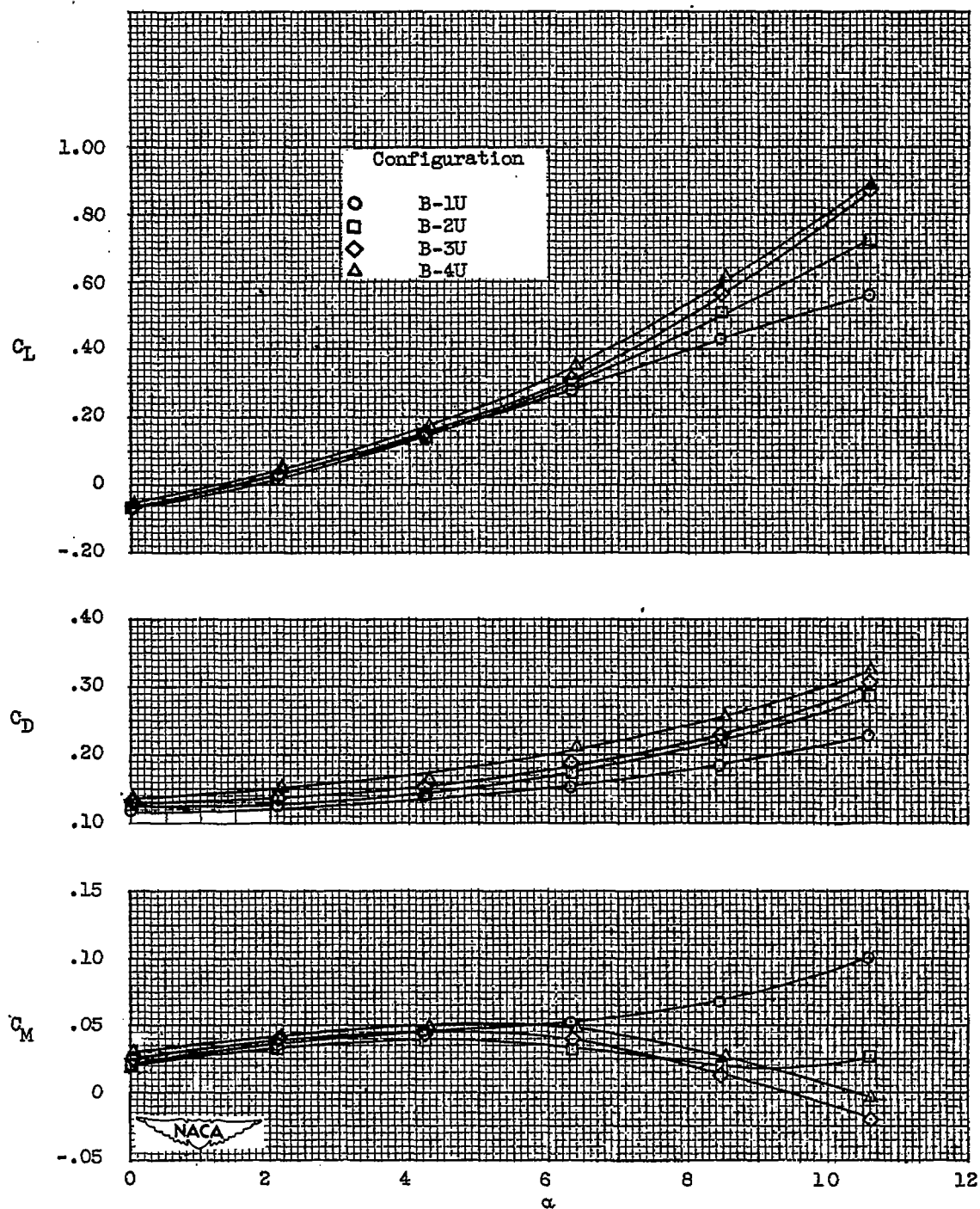
~~CONFIDENTIAL~~(d) Strut center-line position B.  $M_0$ , 2.0.

Figure 6. - Continued. Characteristics of configurations with one engine above body.

~~CONFIDENTIAL~~

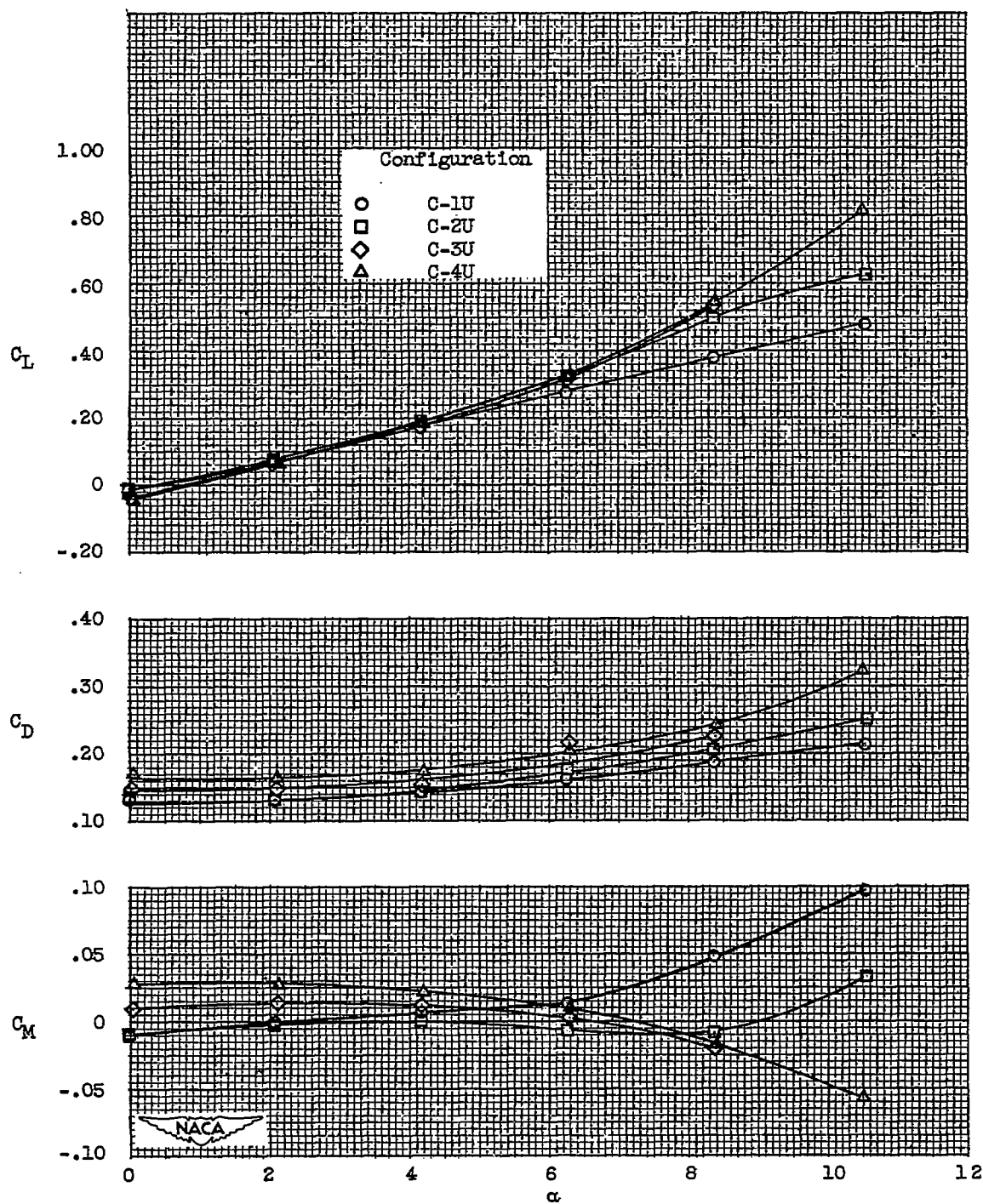
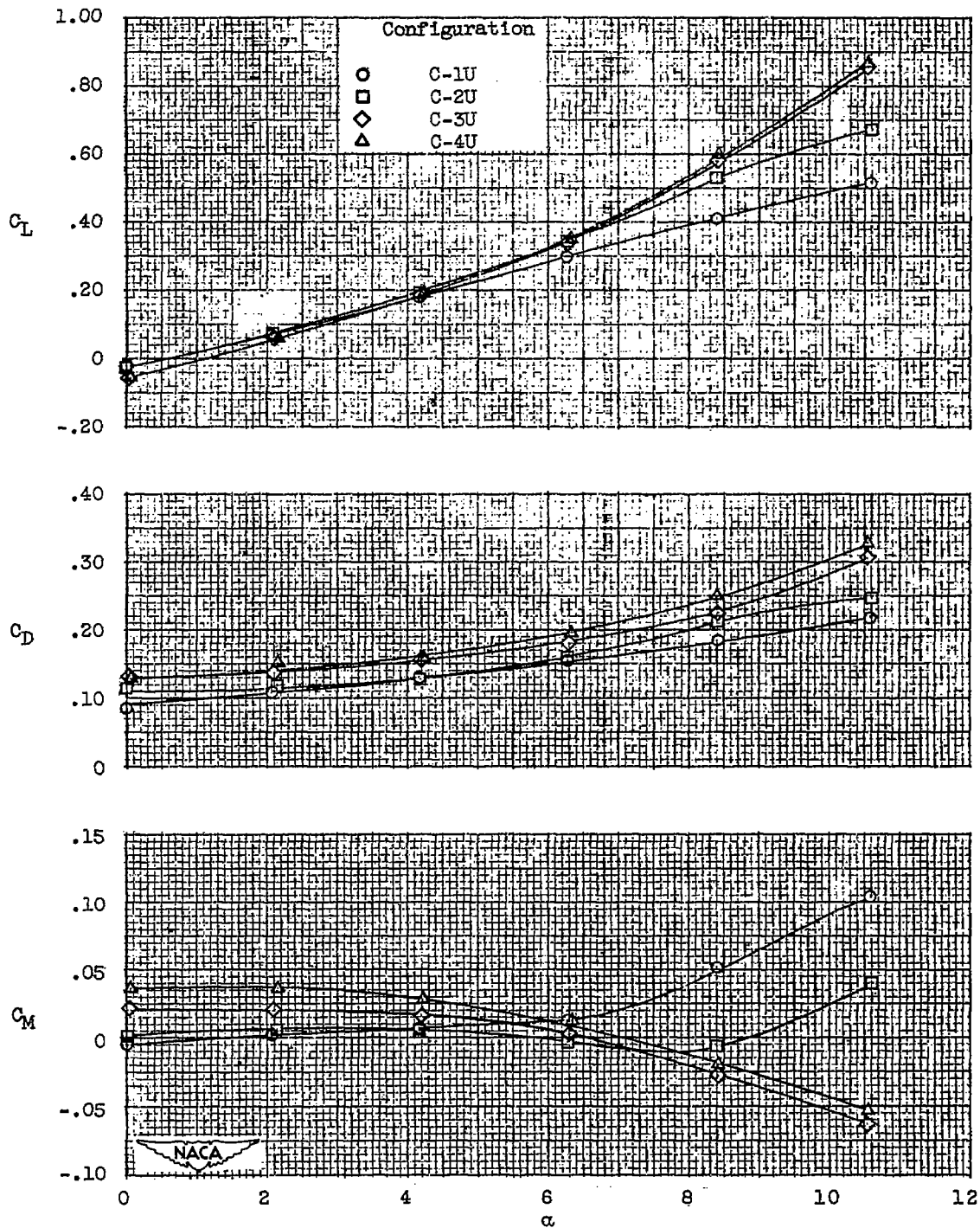
(e) Strut center-line position C.  $M_0$ , 1.8.

Figure 6. - Continued. Characteristics of configurations with one engine above body.



(f) Strut center-line position C.  $M_0$ , 2.0.

Figure 6. - Concluded. Characteristics of configurations with one engine above body.

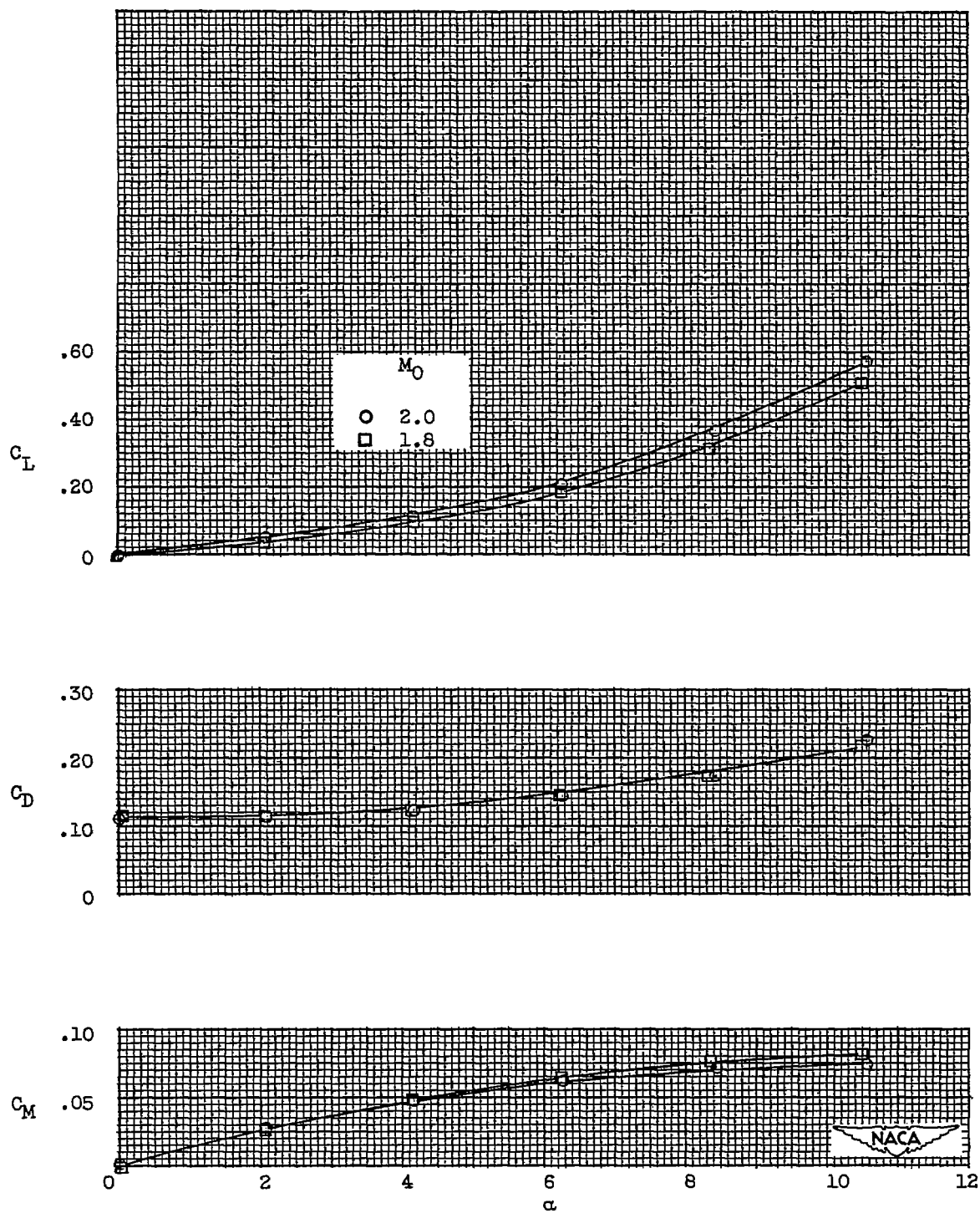


Figure 7. - Characteristics of isolated body.

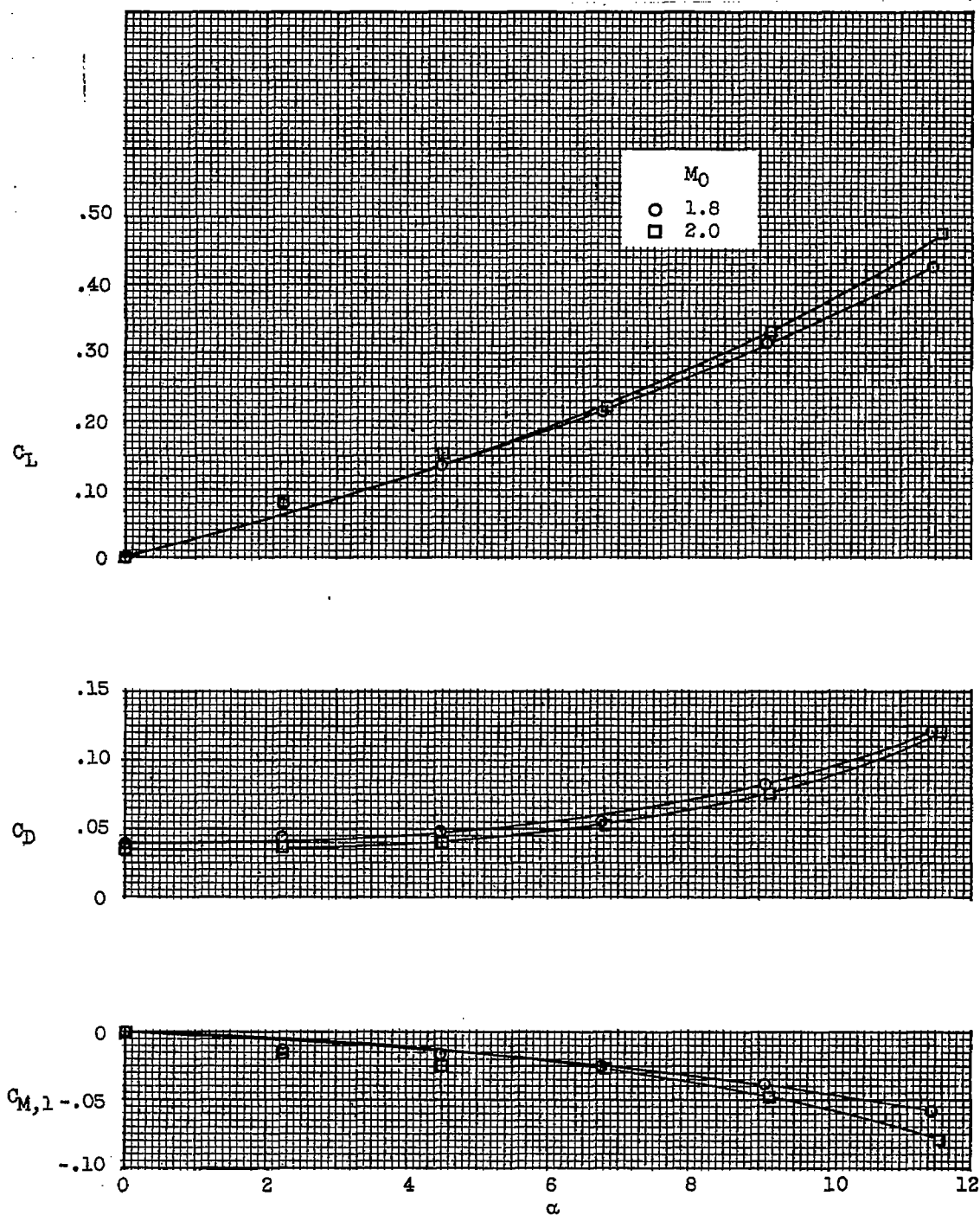


Figure 8. - Characteristics of isolated engine. Coefficients based on body geometry.

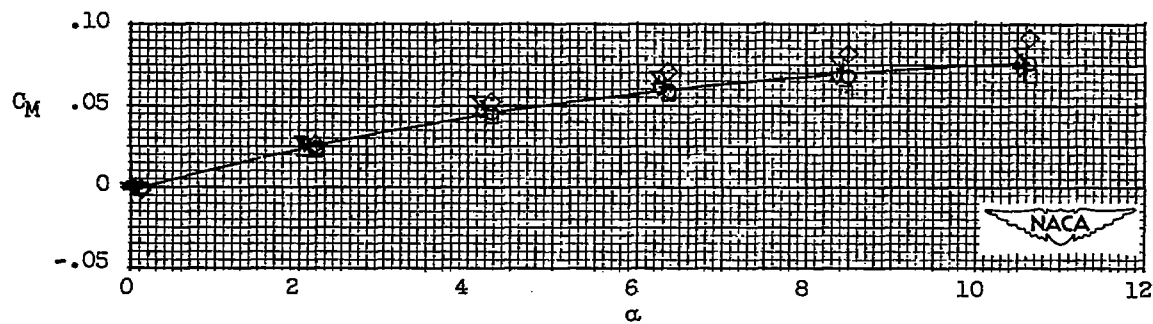
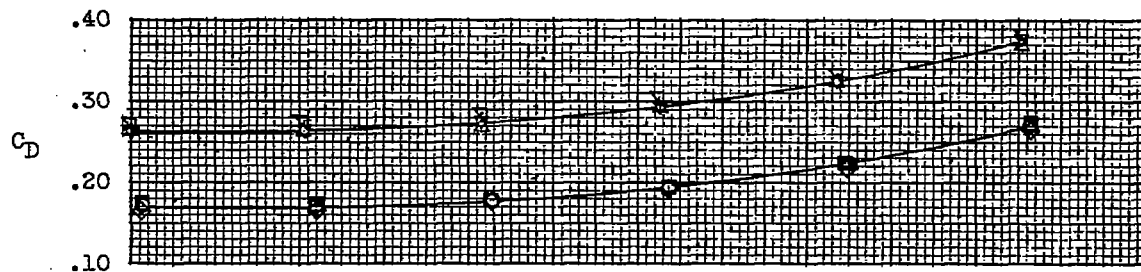
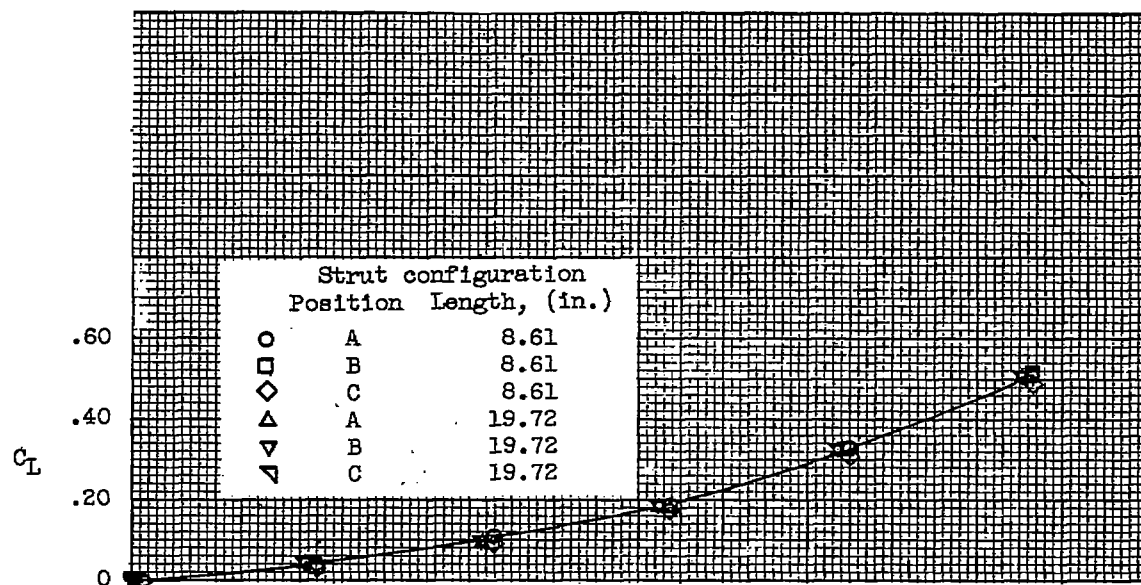
(a)  $M_0, 1.8$ .

Figure 9. - Characteristics of body with two struts.

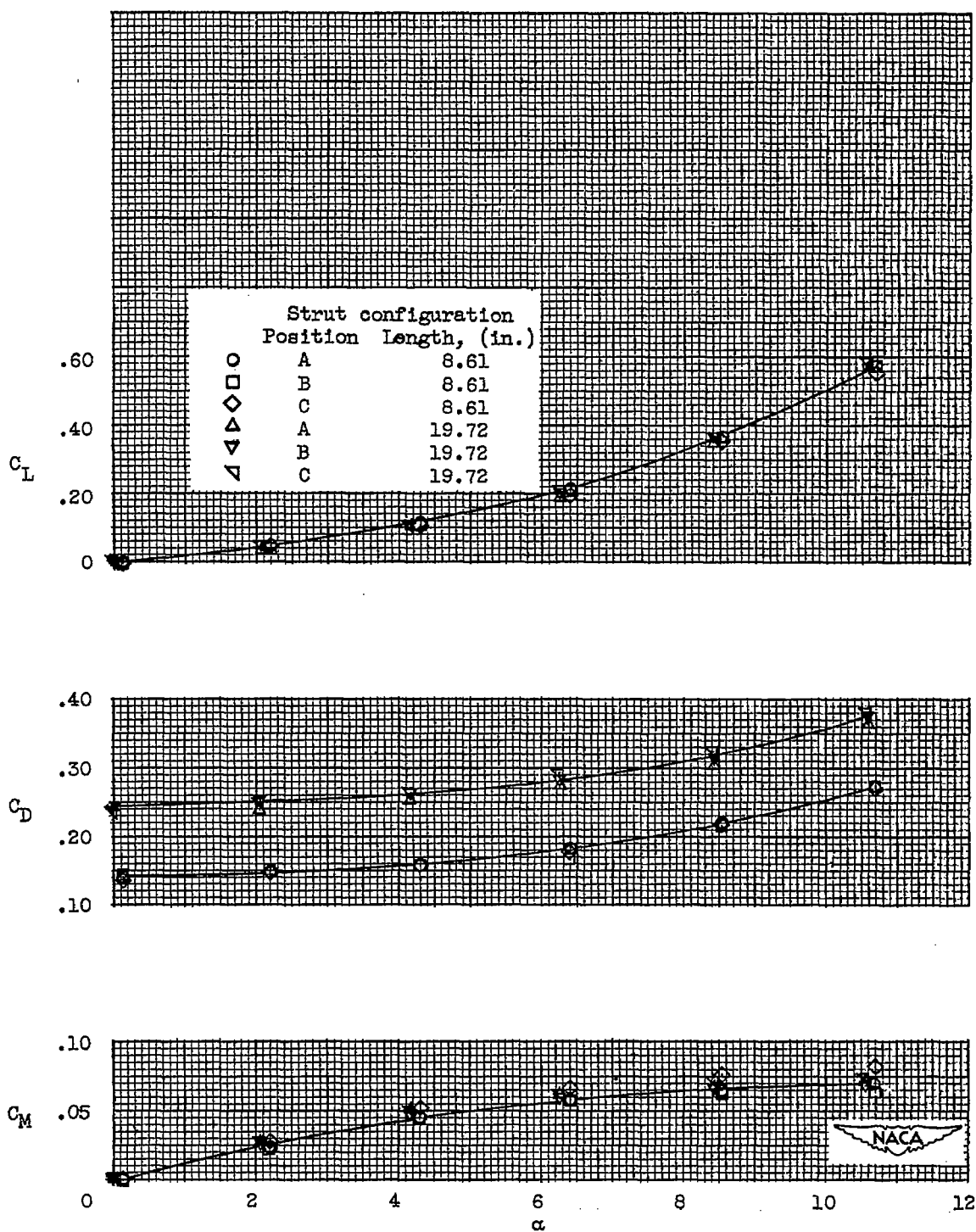


Figure 9. - Concluded. Characteristics of body with two struts.